IBD risk loci are enriched in multigenic regulatory modules encompassing causative genes

Yukihide Momozawa[1,2], Julia Dmitrieva[1*], Emilie Théâtre[1], Valérie Deffontaine[1], Souad Rahmouni[1], Benoît Charloteaux[1], François Crins[1], Elisa Docampo[1], Mahmoud Elansary[1], Ann-Stephan Gori[1], Christelle Lecut[3], Rob Mariman[1], Myriam Mni[1], Cécile Oury[3], Ilya Altukhov[4], Dmitry Alexeev[5], Yuri Aulchenko[6-8], Leila Amininejad[9], G. Bouma[10], F. Hoentjen[11], M. Löwenberg[12], B. Oldenburg[13], M.J. Pierik[14], A.E. van der Meulen-de Jong[15], C.J van der Woude[16], Marijn C Visschedijk[17], The International IBD Genetics Consortium[#], Mark Lathrop[18], Jean-Pierre Hugot[19], Rinse K. Weersma[17], Martine De Vos[20], Denis Franchimont[9], Severine Vermeire[21], Michiaki Kubo[2], Edouard Louis[22], Michel Georges[1].*

[1]Unit of Animal Genomics, WELBIO, GIGA-R & Faculty of Veterinary Medicine, University of Liège (B34), 1 Avenue de l'Hôpital, 4000-Liège, Belgium. [2]Laboratory for Genotyping Development, RIKEN Center for Integrative Medical Science, 1-7-22, Suehiro-cho, Tsurumi-ku, Yokohama, Kanagawa 230-0045, Japan. [3]Laboratory of Thrombosis and Hemostasis, GIGA-R, University of Liège (B34), 1 Avenue de l'Hôpital, 4000-Liège, Belgium. [4]Institute of Physics and Technology, Institutskiy pereulok 9, Dolgoprudny 141700, Russian Federation. [5]Novosibirsk State University, Pirogova ave. 2, 630090 Novosibirsk, Russian Federation, [6]PolyOmica, Het Vlaggeschip 61, 5237 PA, 's-Hertogenbosch, The Netherlands. [7]Institute of Cytology and Genetics SD RAS, Lavrentyeva ave. 10, 630090 Novosibirsk, Russia, [8]Centre for Global Health Research, Usher Institute of Population Health Sciences and Informatics, University of Edinburgh, Teviot Place, Edinburgh, EH8 9AG, UK. [9]Gastroentérologie Médicale, Faculté de Médicine, Université Libre de Bruxelles, Route de Lennik 808, 1070 Anderlecht, Belgium. [10]Department of Gastroenterology and Hepatology, VU University Medical Centre, Amsterdam, The Netherlands. [11] Department of Gastroenterology and Hepatology, University Medical Centre St. Radboud, Nijmegen, The Netherlands. [12]Department of Gastroenterology and Hepatology, Amsterdam Medical Centre, Amsterdam, The Netherlands. [13]Department of Gastroenterology and Hepatology, University Medical Centre Utrecht, Utrecht, The Netherlands. [14]Department of Gastroenterology and Hepatology, University Medical Centre Maastricht, Maastricht, The Netherlands. [15]Department of Gastroenterology and Hepatology, Leiden University Medical Centre, Leiden, The Netherlands. [16]Department of Gastroenterology and Hepatology, Erasmus Medical Centre, the Netherlands, Rotterdam, The Netherlands. [17]Department of Gastroenterology and Hepatology, University of Groningen and University Medical Center Groningen, Hanzeplein 1, 9713 GZ Groningen, The Netherlands. [18]McGill University Centre for Molecular and Computational Genomics, 740 Dr Penfield Avenue, Montreal, Quebec, Canada. [19]UMR 1149 INSERM/Université Paris-Diderot Sorbonne Paris-Cité, Assistance Publique Hôpitaux de Paris, 48 Bd Sérurier, 75019 Paris, France. [20]Department of Gastroenterology, University Hospital, De Pintelaan 185, 9000 Gent, Belgium. [21]Translational Research in Gastrointestinal Disorders, Department of Clinical and Experimental Medicine, KU Leuven, UZ Herestraat 49, 3000 Leuven, Belgium. [22]CHU-Liège and Unit of Gastroenterology, GIGA-R & Faculty of Medicine, University of Liège, 1 Avenue de l'Hôpital, 4000-Liège, Belgium.

[*] Contributed equally.

[#] The complete list of IIBDGC members is provided at the end of the manuscript

Correspondence: michel.georges@ulg.ac.be

GWAS have identified >200 risk loci for Inflammatory Bowel Disease (IBD). The majority of disease associations are known to be driven by regulatory variants. To identify the putative causative genes that are perturbed by these variants, we generate a large transcriptome dataset (9 disease-relevant cell types) and identify 23,650 cis-eQTL. We show that these are determined by ~9,720 regulatory modules, of which ~3,000 operate in multiple tissues and ~970 on multiple genes. We identify regulatory modules that drive the disease association for 63 of the 200 risk loci, and show that these are enriched in multigenic modules. We resequence 45 of the corresponding 100 candidate genes in 6,600 Crohn disease (CD) cases and 5,500 controls and show that they are significantly enriched in causative genes. Our analyses indicate that ≥10-fold larger sample sizes will be required to demonstrate the causality of individual genes using standard burden tests.

INTRODUCTION

Genome Wide Association Studies (GWAS) scan the entire genome for statistical associations between common variants and disease status in large case-control cohorts. GWAS have identified tens to hundreds of risk loci for nearly all studied common complex diseases of human[1]. The study of Inflammatory Bowel Disease (IBD) has been particularly successful, with more than 200 confirmed risk loci reported to date[2,3]. As a result of the linkage disequilibrium (LD) patterns in the human genome (limiting the mapping resolution of association studies), GWAS-identified risk loci typically span ~ 250 kilobases, encompassing an average of ~ 5 genes (numbers ranging from zero ("gene deserts") to more than 50) and hundreds of associated variants. Contrary to widespread misconception, the *causative* variants and genes remain unknown for the vast majority of GWAS-identified risk loci. Yet, this remains a critical goal in order to reap the full benefits of GWAS in identifying new drug targets and developing effective predictive and diagnostic tools. It is the main objective of post-GWAS studies.

Distinguishing the few causative variants (i.e. the variants that are directly causing the gene perturbation) from the many neutral variants that are only

associated with the disease because they are in LD with the former in the studied population, requires the use of sophisticated fine-mapping methods applied to very large, densely genotyped datasets[4], ideally followed-up by functional studies[5]. Using such approaches, 18 causative variants for IBD were recently fine-mapped at single base pair resolution, and 51 additional ones at ≤ 10 base pair resolution[4].

A minority of causative variants are coding, i.e. they alter the amino-acid sequence of the encoded protein. In such cases, and particularly if multiple such causative coding variants are found in the same gene (i.e. in case of allelic heterogeneity), the corresponding causative gene is unambiguously identified. In the case of IBD, causative genes have been identified for ~ ten risk loci on the basis of such "independently" (i.e. not merely reflecting LD with other variants) associated coding variants, including *NOD2*, *ATG16L1*, *IL23R*, *CARD9, FUT2 and TYK2* [4,6-9].

For the majority of risk loci, the GWAS signals are not driven by coding variants. They must therefore be driven by common regulatory variants, i.e. variants that perturb the expression levels of one (or more) target genes in one (or more) disease relevant cell types[4]. Merely reflecting the proportionate sequence space that is devoted to the different layers of gene regulation (transcriptional, posttranscriptional, translational, posttranslational), the majority of regulatory variants are likely to perturb components of "gene switches" (promoters, enhancers, insulators), hence affecting transcriptional output. Indeed, fine-mapped non-coding variants are enriched in known transcription-factor binding sites and epigenetic signatures marking gene switch components[4]. Hence, the majority of common causative variants underlying inherited predisposition to common complex diseases must drive cis-eQTL (expression quantitative trait loci) affecting the causative gene(s) in one or more disease relevant cell types. The corresponding cis-eQTL are expected to operate prior to disease onset, and – driven by common variants – detectable in cohorts of healthy individuals of which most will never develop the disease. The term cis-eQTL refers to the fact that the regulatory variants that drive them only affect the expression of genes/alleles residing on the same DNA molecule, typically no more than one megabase away. Causative variants, whether coding or regulatory, may

secondarily perturb the expression of genes/alleles located on different DNA molecules, generating trans-eQTL. Some of these trans-eQTL may participate in the disease process.

Cis-eQTL effects are known to be very common, affecting more than 50% of genes[10]. Hence, finding that variants associated with a disease are also associated with changes in expression levels of a neighboring gene is not sufficient to incriminate the corresponding genes as causative. Firstly, one has to show that the local association signal for the disease and for the eQTL are driven by the same causative variants. A variety of "colocalisation" methods have been developed to that effect[11-13]. Secondly, regulatory variants may affect elements that control the expression of multiple genes[14], which may not all contribute to the development of the disease, i.e. be causative. Thus, additional evidence is needed to obtain formal proof of gene causality. In humans, the only formal test of gene causality that is applicable is the family of "burden" tests, i.e. the search for a differential burden of disruptive mutations in cases and controls, which is expected only for causative genes[15]. Burden tests rely on the assumption that – in addition to the common, mostly regulatory variants that drive the GWAS signal – the causative gene will be affected by low frequency and rare causative variants, including coding variants. Thus, the burden test makes the assumption that allelic heterogeneity is common, which is supported by the pervasiveness of allelic heterogeneity of Mendelian diseases in humans[16]. Burden tests compare the distribution of rare coding variants between cases and controls[15]. The signal-to-noise ratio of the burden test can be increased by restricting the analysis to coding variants that have a higher probability to disrupt protein function[15]. In the case of IBD, burden tests have been used to prove the causality of *NOD2*, *IL23R* and *CARD9*[6,8,9]. A distinct and very elegant genetic test of gene causality is the reciprocal hemizygosity test, and the related quantitative complementation assay[17,18]. However, with few exceptions[19,20], it has only been applied in model organisms in which gene knock-outs can be readily generated[21].

In this paper, we describe the generation of a new and large dataset for eQTL analysis (350 healthy individuals) in nine cell types that are potentially relevant for IBD. We identify and characterize ~24,000 cis-eQTL. By comparing disease

and eQTL association patterns using a newly developed statistic, we identify 99 strong positional candidate genes in 63 GWAS-identified risk loci. We resequence the 555 exons of 45 of these in 6,600 cases and 5,500 controls in an attempt to prove their causality by means of burden tests. The outcome of this study is relevant to post-GWAS studies of all common complex disease in humans.

RESULTS

Clustering cis-eQTL into regulatory modules

We generated transcriptome data for six circulating immune cell types (CD4+ T lymphocytes, CD8+ T lymphocytes, CD19+ B lymphocytes, CD14+ monocytes, CD15+ granulocytes, platelets) as well as ileal, colonic and rectal biopsies (IL, TR, RE), collected from 323 healthy Europeans (141 men, 182 women, average age 56 years, visiting the clinic as part of a national screening campaign for colon cancer) using Illumina HT12 arrays (CEDAR dataset; Methods). IBD being defined as an inappropriate mucosal immune response to a normal commensal gut flora[22], these nine cell types can all be considered to be potentially disease-relevant. Using standard methods based on linear regression and one megabase windows centered on the position of the interrogating probe (Methods), we identified significant cis-eQTL (FDR < 0.05) for 8,804 of 18,580 tested probes (corresponding to 7,216 of 13,615 tested genes) in at least one tissue, amounting to a total of 23,650 cis-eQTL effects (Supplementary Data 1). When a gene shows a cis-eQTL in more than one tissue, the corresponding "eQTL association patterns" (EAP) (i.e. the distribution of association *-log(p)* values for all the variants in the region of interest) are expected to be similar if determined by the same regulatory variants, and dissimilar otherwise. Likewise, if several neighboring genes show cis-eQTL in the same or distinct tissues, the corresponding EAP are expected to be similar if determined by the same regulatory variants, and dissimilar otherwise (Fig. 1). We devised the ϑ metric to measure the similarity between association patterns (Methods). ϑ is a correlation measure for paired *-log(p)* values (for the two eQTL that are being compared) that ranges between -1 and +1. ϑ shrinks to zero if Pearson's

correlation between paired *-log(p)* values does not exceed a chosen threshold (i.e. if the EAP are not similar). ϑ approaches +1 when the two EAP are similar and when variants that increase expression in eQTL 1 consistently increase expression in eQTL 2. ϑ approaches -1 when the two EAP are similar and when variants that increase expression in eQTL 1 consistently decrease expression in eQTL 2. ϑ gives more weight to variants with high *-log(p)* for at least one EAP (i.e. it gives more weight to eQTL peaks). Based on the known distribution of ϑ under H_0 (i.e. eQTL determined by distinct variants in the same region) and H_1 (i.e. eQTL determined by the same variants), we selected a threshold value $|\vartheta| > 0.60$ to consider that two EAP were determined by the same variant. This corresponds to a false positive rate of 0.05, and a false negative rate of 0.23 (Supplementary Fig. 1). We then grouped EAP in "cis-acting regulatory modules" (cRM) using $|\vartheta|$ and a single-link clustering approach (i.e. an EAP needs to have $|\vartheta| > 0.60$ with at least one member of the cluster to be assigned to that cluster). Clusters were visually examined and 29 single edges connecting otherwise unlinked and yet tight clusters manually removed (Supplementary Fig. 2).

Using this approach, we clustered the 23,650 effects in 9,720 distinct "cis-regulatory modules" (cRM), encompassing cis-eQTL with similar EAP (Supplementary Data 2). Sixty-eight percent of cRM were gene- and tissue-specific, 22% were gene-specific but operating across multiple tissues (≤9 tissues, average 3.5), and 10% were multi-genic (≤11 genes, average 2.5) and nearly always multi-tissue (Fig. 2&3, Supplementary Fig. 2). In this, cRM are considered gene-specific if the EAPs in the cluster concern only one gene, and tissue-specific if the EAP in the cluster concern only one of the nine cell types. They are, respectively, multigenic and multi-tissue otherwise. cRM operating across multiple tissues tended to affect multiple genes ($r = 0.47$; $p < 10^{-6}$). In such cRM, the direction of the effects tended to be consistent across tissues and genes ($p < 10^{-6}$). Nevertheless, we observed at least 55 probes with effect of opposite sign in distinct cell types ($\vartheta \leq -0.9$), i.e. the corresponding regulatory variants increases transcript levels in one cell type while decreasing them in another (Fig. 4 and Supplementary Data 3). Individual tissues allowed for the detection of 7 to 33% of all cRM, and contributed 3 to 14% unique cRM (Supplementary Fig. 3). Sixty-nine percent of cRM were only detected in one cell

type. The rate of cRM sharing between cell types reflects known ontogenic relations. Considering cRM shared by only two cell types (i.e. what jointly differentiates these two cell types from all other), revealed the close proximity of the CD4-CD8, CD14-CD15, ileum-colon, and colon-rectum pairs. Adding information of cRM shared by up to six cell types grouped lymphoid (CD4, CD8, CD19), myeloid (CD14, CD15 but not platelets), and intestinal (ileum, colon and rectum) cells. Adding cRM with up to nine cell types revealed a link between ileum and blood cells, possibly reflecting the presence of blood cells in the ileal biopsies (Fig. 5).

cRM matching IBD association signals are often multigenic

If regulatory variants affect disease risk by perturbing gene expression, the corresponding "disease association patterns" (DAP) and EAP are expected to be similar, even if obtained in distinct cohorts (yet with same ethnicity) (Fig. 6). We confronted DAP and EAP using the ϑ statistic and threshold ($|\vartheta| > 0.60$) described above for 200 GWAS-identified IBD risk loci. DAP for Crohn's disease and Ulcerative Colitis were obtained from the International IBD Genetics Consortium (IIBDGC)[2,3], EAP from the CEDAR dataset.

The probability that two unrelated association signals in a chromosome region of interest are similar (i.e. have high $|\vartheta|$ value) is affected by the degree of LD in the region. If the LD is high it is more likely that two association signals are similar by chance. To account for this, we generated EAP- and locus-specific distributions of $|\vartheta|$ by simulating eQTL explaining the same variance as the studied eQTL, yet driven by 100 variants that were randomly selected in the risk locus (matched for MAF), and computing $|\vartheta|$ with the DAP for all of these. The resulting empirical distribution of $|\vartheta|$ was used to compute the probability to obtain a value of $|\vartheta|$ as high or higher than the observed one, by chance alone (Methods).

Strong correlations between DAP and EAP ($|\vartheta| > 0.6$, associated with low empirical p-values) were observed for at least 63 IBD risk loci, involving 99 genes (range per locus: 1-6) (Table 1, Fig. 7, Supplementary Data 4). Increased disease risk was associated equally frequently with increased as with decreased expression (p_{CD} = 0.48; p_{UC} = 0.88). An open-access website has been prepared

to visualize correlated DAP-EAP within their genomic context (http://cedar-web.giga.ulg.ac.be). Genes with highest $|\vartheta|$ values (≥ 0.9) include known IBD causative genes (f.i. *ATG16L1*, *CARD9, FUT2*), known immune regulators (f.i. *IL18R1, IL6ST, THEMIS*), as well as genes with as of yet poorly defined function in the context of IBD (f.i. *APEH, ANKRD55*, *CISD1, CPEB4, DOCK7, ERAP2*, *GNA12*, *GPX1, GSDMB, ORMDL3, SKAP2*, *UBE2L3, ZMIZ1*) (Supplementary Note 1).

The eQTL link with IBD has not been reported before for at least 47 of the 99 reported genes (Table 1). eQTL links with IBD have been previously reported for 111 additional genes, not mentioned in Table 1. Our data support these links for 19 of them, however, with $|\vartheta| \leq 0.6$ (Supplementary Data 5). We applied SMR[13] as alternative colocalisation method to our data. Using a Bonferroni-corrected threshold of $\leq 2.5 \times 10^{-5}$ for p_{SMR} and ≥ 0.05 for p_{HEIDI}, SMR detected 35 of the 99 genes selected with ϑ (Supplementary Data 4). Using the same thresholds, SMR detected nine genes that were not selected by ϑ. Of these, three (*ADAM15*, *AHSA2*, *UBA7*) had previously been reported by others, while six (*FAM189B, QRICH1, RBM6, TAP2, ADO, LGALS9*) were not. Of these six, three (*RBM6*, *TAP2*, *ADO*) were characterized by $0.45 < |\vartheta| < 0.6$ (Supplementary Data 5).

Using an early version of the CEDAR dataset, significant (albeit modest) enrichment of overlapping disease and eQTL signals was reported for CD4, ileum, colon and rectum, focusing on 76 of 97 studied IBD risk loci (MAF of disease variant > 0.05)[4]. By pre-correcting fluorescence intensities with 23 to 53 (depending on cell type) principal components to account for unidentified confounders (Methods), we increased the number of significant eQTL from 480 to 880 in the corresponding 97 regions (11,964 to 23,650 for the whole genome). We repeated the enrichment analysis focusing on 63 of the same 97 IBD loci (CD risk loci; MAF of disease variant > 0.05), using three colocalisation methods including ϑ (Methods). We observed a systematic excess overlap in all analyzed cell types (2.5-fold on average). The enrichment was very significant with the three methods in CD4 and CD8 (Supplementary Table 1).

The 400 analyzed DAP (200 CD and 200 UC) were found to match 76 cRM (in 63 risk loci) with $|\vartheta| > 0.6$ (Table 1), of which 25 are multigenic. Knowing that multigenic cRM represent 10% of all cRM (967/9,720), 25/76 (i.e. 33%)

corresponds to a highly significant 3-fold enrichment ($p < 10^{-9}$). To ensure that this apparent enrichment was not due to the fact that multigenic cRM have more chance to match DAP (as by definition multiple EAP are tested for multigenic cRM), we repeated the enrichment analysis by randomly sampling only one representative EAP per cRM in the 200 IBD risk loci. The frequency of multigenic cRM amongst DAP-matching cRM averaged 0.22, and was never ≤ 0.10 ($p \leq 10^{-5}$) (Supplementary Fig. 4). In loci with high LD, EAP driven by distinct regulatory variants (yet in high LD) may erroneously be merged in the same cRM. To ensure that the observed enrichment in multigenic cRM was not due to higher levels of LD, we compared the LD-based recombination rate of the 63 cRM-matching IBD risk loci with that of the rest of the genome[23]. The genome-average recombination rate was 1.23 centimorgan per megabase (cM/Mb), while that of the 63 IBD risk loci was 1.34 cM/Mb, i.e. less LD in the 63 cRM-matching IBD risk loci than in the rest of the genome. We further compared the average recombination rate in the 63 cRM-matching IBD regions with that of sets of 63 loci centered on randomly drawn cRM (from the list of 9,720), matched for size and chromosome number (as cM/Mb is affected by chromosome size). The average recombination rate around all cRM was 1.43 cM/Mb, and this didn't differ significantly from the 63 cRM-matching IBD regions (p=0.46) (Supplementary Fig. 5). Therefore, the observed enrichment cannot be explained by a higher LD in the 63 studied IBD risk loci. Taken together, EAP that are strongly correlated with DAP ($|\vartheta| \geq 0.60$), map to regulatory modules that are 2- to 3-fold enriched in multigenic cRM when compared to the genome average and include four of the top 10 (of 9,720) cRM ranked by number of affected genes.

DAP-matching cRM are enriched in causative genes for IBD

For truly causative genes, the burden of rare disruptive variants is expected to differ between cases and controls[24]. We therefore performed targeted sequencing for the 555 coding exons (~88 Kb) of 38 genes selected amongst those with strongest DAP-EAP correlations, plus seven genes with suggestive DAP-EAP evidence backed by literature (Table 1), in 6,597 European CD cases and 5,502 matched controls (ref. 25 and Methods). Eighteen of these were part of single-gene cRM and the only gene highlighted in the corresponding locus. The

306 remaining 27 corresponded to multi-gene cRM mapping to 15 risk loci. We
307 added the well-established *NOD2* and *IL23R* causative IBD genes as positive
308 controls. We identified a total of 174 loss-of-function (LoF) variants, 2,567
309 missense variants (of which 991 predicted by SIFT[26] to be damaging and
310 Polyphen-2[27] to be either possibly or probably damaging), and 1,434
311 synonymous variants (Fig. 8 and Supplementary Data 6). 1,781 of these were
312 also reported in the Genome Aggregation Database[28] with nearly identical allelic
313 frequencies (Supplementary Fig. 6). We designed a gene-based burden test to
314 simultaneously evaluate hypothesis (i): all disruptive variants enriched in cases
315 (when $\vartheta < 0$; risk variants) or all disruptive variants enriched in controls (when ϑ
316 > 0; protective variants), and hypothesis (ii): some disruptive variants enriched
317 in cases and others in controls. Hypothesis (i) was tested with CAST[29], and
318 hypothesis (ii) with SKAT[30] (Methods). We restricted the analysis to 1,141 LoF
319 and damaging missense variants with minor allele frequency (MAF) ≤ 0.005 to
320 ensure that any new association signal would be independent of the signals from
321 common and low frequency variants having led to the initial identification and
322 fine-mapping of the corresponding loci[4]. For *NOD2* ($p = 6.9 \times 10^{-7}$) and *IL23R* ($p = 1.8 \times 10^{-4}$), LoF and damaging variants were significantly enriched in
324 respectively cases and controls as expected. When considering the 45 newly
325 tested genes as a whole, we observed a significant ($p = 6.9 \times 10^{-4}$) shift towards
326 lower p-values when compared to expectation, while synonymous variants
327 behaved as expected ($p = 0.66$) (Fig. 9 and Supplementary Data 7). This strongly
328 suggests that the sequenced list includes causative genes. *CARD9*, *TYK2* and
329 *FUT2* have recently been shown to be causative genes based on disease-
330 associated low-frequency coding variants (MAF > 0.005)[4]. The shift towards
331 lower p-values remained significant without these ($p = 1.7 \times 10^{-3}$), pointing
332 towards novel causative genes amongst the 42 remaining candidate genes.

333 ***Proving gene causality requires larger case-control cohorts.***

334 Despite the significant shift towards lower p-values when considering the 45
335 genes jointly, none of these were individually significant when accounting for
336 multiple testing ($p \leq \frac{0.05}{2*45} \approx 0.0006$) (Supplemental Data 7). Near identical
337 results were obtained when classifying variants using the Combined Annotation

Dependent Depletion (CADD) tool[31] instead of SIFT/PolyPhen-2 (Supplementary Data 7). We explored three approaches to increase the power of the burden test. The first built on the observation that cRM matching DAP are enriched in multigenic modules. This suggests that part of IBD risk loci harbor multiple co-regulated and hence functionally related genes, of which several (rather than one, as generally assumed) may be causally involved in disease predisposition. To test this hypothesis, we designed a module- rather than gene-based burden test (Methods). However, none of the 30 tested modules reached the experiment-wide significance threshold ($p \leq \frac{0.05}{2*30} \approx 0.0008$). Moreover, the shift towards lower p-values for the 30 modules was not more significant ($p = 2.3\ x\ 10^{-3}$) than for the gene-based test (Supplementary Fig. 7A and Supplementary Table 7). The second and third approaches derive from the common assumption that the heritability of disease predisposition may be larger in familial and early-onset cases[32]. We devised orthogonal tests for age-of-onset and familiality and combined them with our burden tests (Methods). Neither approach would improve the results (Supplementary Fig. 7B&C and Supplementary Data 7).

Assuming that *TYK2* and *CARD9* are truly causative and their effect sizes in our data unbiased, we estimated that a case-control cohort ranging from ~ 50,000 (*TYK2*) to ~200,000 (*CARD9*) individuals would have been needed to achieve experiment-wide significance (testing 45 candidate genes), and from ~ 78,000 (*TYK2*) to >500,000 (*CARD9*) individuals to achieve genome-wide significance (testing 20,000 genes) in the gene-based burden test (Supplementary Fig. 8).

DISCUSSION

We herein describe a novel dataset comprising array-based transcriptome data for six circulating immune cell types and intestinal biopsies at three locations collected on ~300 healthy European individuals. We use this CEDAR dataset ("Correlated Expression and Disease Association Research") to identify 23,650 significant cis-eQTL, which fall into 9,720 regulatory modules of which at least ~889 affect more than one gene in more than one tissue. We provide strong evidence that 63 of 200 known IBD GWAS signals reflect the activity of common

regulatory variants that preferentially drive multigenic modules. We perform an exon-based burden test for 45 positional candidate CD genes mapping to 33 modules, in 5,500 CD cases and 6,500 controls. By demonstrating a significant ($p = 6.9\ x\ 10^{-4}$) upwards shift of log(1/p) values for damaging when compared to synonymous variants, we show that the sequenced genes include new causative CD genes.

Individually, none of the sequenced genes (other than the positive *NOD2* and *IL23R* controls) exceed the experiment-wide significance threshold, precluding us from definitively pinpointing any novel causative genes. However, we note *IL18R1* amongst the top-ranking genes (see also Supplementary Note 1). *IL18R1* is the only gene in an otherwise relatively gene-poor region (also encompassing *IL1R1* and *IL18RAP*) characterized by robust cis-eQTL in CD4 and CD8 that are strongly correlated with the DAP for CD and UC ($0.68 \leq |\vartheta| \leq 0.93$). Reduced transcript levels of *IL18R1* in these cell types is associated with increased risk for IBD. Accordingly, rare (MAF ≤ 0.005) damaging variants were cumulatively enriched in CD cases (CAST p = 0.05). The cumulative allelic frequency of rare damaging variants was found to be higher in familial CD cases (0.0027), when compared to non-familial CD cases (0.0016; p = 0.09) and controls (0.0010; p = 0.03). When ignoring carriers of deleterious *NOD2* mutations, average age-of-onset was reduced by ~3 years (25.3 vs 28.2 years) for carriers of rare damaging *IL18R1* variants but this difference was not significant (p = 0.18).

While the identification of matching cRM for 63/200 DAP points towards a number of strong candidate causative genes, it leaves most risk loci without matching eQTL despite the analysis of nine disease-relevant cell types. This finding is in agreement with previous reports[4,33]. It suggests that cis-eQTL underlying disease predisposition operate in cell types, cell states (f.i. resting vs activated) or developmental stages that were not explored in this and other studies. It calls for the enlargement and extension of eQTL studies to more diverse and granular cellular panels[10,34], possibly by including single-cell sequencing or spatial transcriptomic approaches. By performing eQTL studies in a cohort of healthy individuals, we have made the reasonable assumption that the common regulatory variants that are driving the majority of GWAS signals are acting before disease onset, including in individuals that will never develop

the disease. An added advantage of studying a healthy cohort, is that the corresponding dataset is "generic", usable for the study of perturbation of gene regulation for any common complex disease. However, it is conceivable that some eQTL underlying increased disease risk only manifest themselves once the disease process is initiated, for instance as a result of a modified inflammatory status. Thus, it may be useful to perform eQTL studies with samples collected from affected individuals to see in how far the eQTL landscape is affected by disease status.

One of the most striking results of this work is the observation that cRM that match DAP are ≥2-fold enriched in multi-genic modules. We cannot fully exclude that this is due to ascertainment bias. As multi-genic modules tend to also be multi-tissue, multi-genic cRM matching a DAP in a non-explored disease-relevant cell type have a higher probability to be detected in the explored cell types than the equivalent monogenic (and hence more likely cell type specific) cRM. The alternative explanation is that cRM matching DAP are truly enriched in multi-genic cRM. It is tempting to surmise that loci harboring clusters of co-regulated, functionally related causative genes have a higher probability to be detected in GWAS, reflecting a relatively larger target space for causative mutations. We herein tested this hypothesis by applying a module rather than gene-based test. Although this did not appear to increase the power of the burden test in this work, it remains a valuable approach to explore in further studies. Supplementary Data 2 provides a list of >900 multigenic modules detected in this work that could be used in this context.

Although we re-sequenced the ORF of 45 carefully selected candidate genes in a total of 5,500 CD cases and 6,600 controls, none of the tested genes exceeded the experiment-wide threshold of significance. This is despite the fact that we used a one-sided, eQTL-informed test to potentially increase power. Established IBD causative genes used as positive control, *NOD2* and *IL23R*, were positive indicating that the experiment was properly conducted. We were not able to improve the signal strength by considering information about regulatory modules, familiality or age-of-onset. We estimated that ≥10-fold larger sample sizes will be needed to achieve adequate power if using the same approach.

Although challenging, these numbers are potentially within reach of international consortia for several common diseases including IBD.

It is conceivable that the organ-specificity of nearly all complex diseases (such as the digestive tract for IBD), reflects tissue-specific perturbation of broadly expressed causative genes that may fulfill diverse functions in different organs. If this is true, coding variants may not be the appropriate substrate to perform burden tests, as these will affect the gene across all tissues. In such instances, the disruptive variants of interest may be those perturbing tissue-specific gene switches. Also, it has recently been proposed that the extreme polygenic nature of common complex diseases may reflect the trans-effects of a large proportion of regulatory variants active in a given cell type on a limited number of core genes via perturbation of highly connected gene networks[35]. Identifying rare regulatory variants is still challenging, however, as tissue-specific gene switches remain poorly catalogued, and the effect of variants on their function difficult to predict. The corresponding sequence space may also be limited in size, hence limiting power. Nevertheless, a reasonable start may be to re-sequence the regions surrounding common regulatory variants that have been fine-mapped at near single base pair resolution[4].

In conclusion, we hereby provide to the scientific community a collection of ~24,000 cis-eQTL in nine cell types that are highly relevant for the study of inflammatory and immune-mediated diseases, particularly of the intestinal tract. The CEDAR dataset advantageously complements existing eQTL datasets including GTEx[10,34]. We propose a paradigm to rationally organize cis-eQTL effects in co-regulated clusters or regulatory modules. We identify ~100 candidate causative genes in 63 out of 200 analyzed risk loci, on the basis of correlated DAP and EAP. We have developed a web-based browser to share the ensuing results with the scientific community (http://cedar-web.giga.ulg.ac.be). The CEDAR website will imminently be extended to accommodate additional common complex disease for which GWAS data are publicly available. We show that the corresponding candidate genes are enriched in causative genes, however, that case-control cohorts larger than those used in this study (12,000 individuals) are required to formally demonstrate causality by means of presently available burden tests.

METHODS

Sample collection in the CEDAR cohort

We collected peripheral blood as well as intestinal biopsies (ileum, transverse colon, rectum) from 323 healthy Europeans visiting the Academic Hospital of the University of Liège as part of a national screening campaign for colon cancer. Participants included 182 women and 141 men, averaging 56 years of age (range: 19-86). Enrolled individuals were not suffering any autoimmune or inflammatory disease and were not taking corticosteroids or non-steroid anti-inflammatory drugs (with the exception of low doses of aspirin to prevent thrombosis). We recorded birth date, weight, height, smoking history, declared ethnicity and hematological parameters (red blood cell count, platelet count, differential white blood cell count) for each individual. The experimental protocol was approved by the ethics committee of the University of Liège Academic Hospital. Informed consent was obtained prior to donation in agreement with the recommendations of the declaration of Helsinki for experiments involving human subjects. We refer to this cohort as CEDAR for Correlated Expression and Disease Association Research.

SNP genotyping and imputation

Total DNA was extracted from EDTA-collected peripheral blood using the MagAttract DNA blood Midi M48 Kit on a QIAcube robot (Qiagen). DNA concentrations were measured using the Quant-iT Picogreen ds DNA Reagents (Invitrogen). Individuals were genotyped for > 700K SNPs using Illumina's Human OmniExpress BeadChips, an iScan system and the Genome Studio software following the guidelines of the manufacturer. We eliminated variants with call rate ≤ 0.95, deviating from Hardy-Weinberg equilibrium ($p \leq 10^{-4}$), or which were monomorphic. We confirmed European ancestry of all individuals by PCA using the HapMap population as reference. Using the real genotypes of 629,570 quality-controlled autosomal SNPs as anchors, we used the Sanger Imputation Services with the UK10K + 1,000 Genomes Phase 3 Haplotype panels[43-46] to impute genotypes at autosomal variants in our population. We

eliminated indels, SNPs with MAF ≤ 0.05, deviating from Hardy-Weinberg equilibrium ($p \leq 10^{-3}$), and with low imputation quality (INFO ≤ 0.4), leaving 6,019,462 high quality SNPs for eQTL analysis.

Transcriptome analysis

Blood samples were kept on ice and treated within one hour after collection as follows. EDTA-collected blood was layered on Ficoll-Paque PLUS (GE Healthcare) to isolate peripheral blood mononuclear cells by density gradient centrifugation. CD4+ T lymphocytes, CD8+ T lymphocytes, CD19+ B lymphocytes, CD14+ monocytes, CD15+ granulocytes were isolated by positive selection using the MACS technology (Miltenyi Biotec). To isolate platelets, blood collected on acid-citrate-dextrose (ACD) anticoagulant was centrifuged at 150g for 10 minutes. The platelet rich plasma (PRP) was collected, diluted 2-fold in ACD buffer and centrifuged at 800g for 10 minutes. The platelet pellet was resuspended in MACS buffer (Miltenyi Biotec) and platelets purified by negative selection using CD45 microbeads (Miltenyi Biotec). Intestinal biopsies were flash frozen in liquid nitrogen immediately after collection and kept at -80°C until RNA extraction. Total RNA was extracted from the purified leucocyte populations and intestinal biopsies using the AllPrep Micro Kit and a QIAcube robot (Qiagen). For platelets, total RNA was extracted manually with the RNeasy Mini Kit (Qiagen). Whole genome expression data were generated using HT-12 Expression Beadchips following the instructions of the manufacturer (Illumina). Technical outliers were removed using controls recommended by Illumina and the Lumi package[47]. We kept 29,464/47,323 autosomal probes (corresponding to 19,731 genes) mapped by Re-Annotator[48] to a single gene body with ≤ 2 mismatches and not spanning known variants with MAF > 0.05. Within cell types, we only considered probes (i.e. "usable" probes) with detection p-value ≤ 0.05 in ≥ 25% of the samples. Fluorescence intensities were Log_2 transformed and Robust Spline Normalized (RSN) with Lumi[47]. Normalized expression data were corrected for sex, age, smoking status and Sentrix Id using ComBat from the SVA R library[49]. We further corrected the ensuing residuals within tissue for the number of Principal Components (PC) that maximized the number of cis-eQTL with $p \leq 10^{-6}$ [50]. Supplementary Table 2 summarizes the number of usable samples, probes and PC for each tissue type.

Cis-eQTL analysis

Cis-eQTL analyses were conducted with PLINK and using the expression levels precorrected for fixed effects and PC as described above[51,52]. Analyses were conducted under an additive model, i.e. assuming that the average expression level of heterozygotes is at the midpoint between alternate homozygotes. To identify cis-eQTL we tested all SNPs in a 2Mb window centered around the probe (if "usable"). P-values for individual SNPs were corrected for the multiple testing within the window by permutation (10,000 permutations). For each probe-tissue combination we kept the best (corrected) p-value. Within each individual cell type, the ensuing list of corrected p-values was used to compute the corresponding false discovery rates (FDR or q-value). Supplementary Table 3 reports the number of cis-eQTL found in the nine analyzed cell types for different FDR thresholds (see also Supplementary Figure 9).

Comparing EAP with ϑ to identify cis Regulatory Modules

If the transcript levels of a given gene are influenced by the same regulatory variants (one or several) in two tissues, the corresponding EQTL Association Patterns (EAP)(i.e. the -log(p) values of association for the SNPs surrounding the gene) are expected to be similar. Likewise, if the transcript levels of different genes are influenced by the same regulatory variants in the same or in different tissues, the corresponding EAP are expected to be similar (cfr. main text, Fig. 1). We devised a metric, ϑ, to quantify the similarity between EAP. If two EAP are similar, one can expect the corresponding –log(p) values to be positively correlated. One particularly wants the EAP peaks, i.e. the highest -log(p) values, to coincide in order to be convinced that the corresponding cis-eQTL are driven by the same regulatory variants. To quantify the similarity between EAP while emphasizing the peaks we developed a weighted correlation. Imagine two vectors **X** and **Y** of –log(p) values for *n* SNPs surrounding the gene(s) of interest. Using the same nomenclature as in Fig. 1A, **X** could correspond to gene A in tissue 1, and **Y** to gene A in tissue 2, or **X** could correspond to gene A in tissue 1, and **Y** to gene B in tissue 2. We only consider for analysis, SNPs within 1Mb of either gene (probe) and for which x_i and/or y_i is superior to 1.3 (i.e. p-value < 0.05) hence informative for at least one of the two cis-eQTL. Indeed, the

majority of variants with –log(p) < 1.3 (p > 0.05) for both EAP are by definition not associated with either trait. There is therefore no reason to expect that they could contribute useful information to the correlation metric: their ranking in terms of –log(p) values becomes more and more random as the –log(p) decreases. We define the weight to be given to each SNP in the correlation as:

$$w_i = \left(MAX\left(\frac{x_i}{x_{MAX}}, \frac{y_i}{y_{MAX}}\right)\right)^p$$

The larger *p*, the more weight is given to the top SNPs. In this work, *p* was set at one.

The weighted correlation between the two EAP, r_w, is then computed as:

$$r_w = \frac{1}{\sum_{i=1}^{n} w_i} \sum_{i=1}^{n} w_i \left(\frac{x_i - \overline{x_w}}{\sigma_x^w}\right)\left(\frac{y_i - \overline{y_w}}{\sigma_y^w}\right)$$

in which

$$\overline{x_w} = \frac{\sum_{i=1}^{n} w_i \times x_i}{\sum_{i=1}^{n} w_i}$$

$$\overline{y_w} = \frac{\sum_{i=1}^{n} w_i \times y_i}{\sum_{i=1}^{n} w_i}$$

$$\sigma_x^w = \sqrt{\frac{\sum_{i=1}^{n} w_i \times (x_i - \overline{x_w})^2}{\sum_{i=1}^{n} w_i}}$$

$$\sigma_y^w = \sqrt{\frac{\sum_{i=1}^{n} w_i \times (y_i - \overline{y_w})^2}{\sum_{i=1}^{n} w_i}}$$

The larger r_w, the larger the similarity between the EAP, particularly for their respective peak SNPs.

r_w ignores an important source of information. If two EAP are driven by the same regulatory variant, there should be consistency in the signs of the effects across SNPs in the region. We will refer to the effect of the "reference" allele of SNP *i* on the expression levels for the first and second cis-eQTL as β_i^X and β_i^Y. If the

reference allele of the regulatory variant increases expression for both cis-eQTL, the β_i^X and β_i^Y's for a SNPs in LD with the regulatory variant are expected to have the same sign (positive or negative depending on the sign of D for the considered SNP). If the reference allele of the regulatory variant increases expression for one cis-eQTL and decreases expression for the other, the β_i^X and β_i^Y's for a SNPs in LD with the regulatory variant are expected to have opposite sign. We used this notion to develop a weighted and signed measure of correlation, r_{ws}. The approach was the same as for r_w, except that the values of y_i were multiplied by -1 if the signs of β_i^X and β_i^Y were opposite. r_{ws} is expected to be positive if the regulatory variant affects the expression of both cis-eQTL in the same direction and negative otherwise.

We finally combined r_w and r_{ws} in a single score referred to as ϑ, as follows:

$$\vartheta = \frac{r_{ws}}{1 + e^{-k(r_w - T)}}$$

ϑ penalizes r_{ws} as a function of the value of r_w. The aim is to avoid considering EAP pairs with strong but negative r_w (which is often the case when the two EAP are driven by very distinct variants). The link function is a sigmoid-shaped logistic function with k as steepness parameter and T as sigmoid mid-point. In this work, we used a value of k of 30, and a value of T of 0.3 (Supplementary Figure 10).

We first evaluated the distribution of ϑ for pairs of EAP driven by the same regulatory variants by studying 4,693 significant cis-eQTL (FDR < 0.05). For these, we repeatedly (100 x) split our CEDAR population in two halves, performed the cis-eQTL analysis separately on both halves and computed ϑ for the ensuing EAP pairs. Supplementary Figure 1 is showing the obtained results.

We then evaluated the distribution of ϑ for pairs of EAP driven by distinct regulatory variants in the same chromosomal region as follows. We considered 1,207 significant cis-eQTL (mapping to the 200 IBD risk loci described above). For each one of these, we generated a set of 100 "matching" cis-eQTL effects in silico, sequentially considering 100 randomly selected SNPs (from the same locus) as causal. The in silico cis-eQTL were designed such that they would explain the same fraction of expression variance as the corresponding real cis-

609 eQTL detected with PLINK (cfr. above). When performing cis-eQTL analysis
610 under an additive model, PLINK estimates β_0 (i.e. the intercept), and β_1 (i.e. the
611 slope of the regression), including for the top SNP. Assume that the expression
612 level of the studied gene, Z, for individual i is z_i. Assume that the sample
613 comprises n_T individuals in total, of which n_{11} are of genotype "*11*", n_{12} of
614 genotype "*12*", and n_{22} of genotype "*22*", for the top cis-eQTL SNP. The total
615 expression variance for gene Z equals:

$$\sigma_T^2 = \frac{\sum_{i=1}^{n_T}(z_i - \overline{z_T})^2}{n_T - 1}$$

616 The variance in expression level due to the cis-eQTL equals:

$$\sigma_{eQTL}^2 = \frac{n_{11}(\beta_0 - \overline{z_T})^2 + n_{12}(\beta_0 + \beta_1 - \overline{z_T})^2 + n_{22}(\beta_0 + 2\beta_1 - \overline{z_T})^2}{n_T}$$

617 The heritability of expression due to the cis-eQTL, i.e. the fraction of the
618 expression variance that is due to the cis-eQTL is therefore:

$$h_{eQTL}^2 = \frac{\sigma_{eQTL}^2}{\sigma_T^2}$$

619 To simulate cis-eQTL explaining the same h_{eQTL}^2 as the real eQTL in the CEDAR
620 dataset, we sequentially considered all SNPs in the region. Each one of these
621 SNPs would be characterized by n_{11} individuals of genotype "*11*", n_{12} of genotype
622 "*12*", and n_{22} of genotype "*22*", for a total of n_T genotyped individuals. We would
623 arbitrarily set $\overline{z_{11}}$, $\overline{z_{12}}$, and $\overline{z_{22}}$ at -1, 0 and +1. As a consequence, the variance
624 due to this cis-eQTL equals:

$$\sigma_{eQTL}^2 = \frac{n_{11}(-1 - \overline{z_T})^2 + n_{12}(0 - \overline{z_T})^2 + n_{22}(1 - \overline{z_T})^2}{n_T}$$

625 in which $\overline{z_T} = (n_{22} - n_{11})/n_T$.

626 Knowing σ_{eQTL}^2 and h_{eQTL}^2, and knowing that

$$h_{eQTL}^2 = \frac{\sigma_{eQTL}^2}{\sigma_{eQTL}^2 + \sigma_{RES}^2}$$

627 the residual variance σ_{RES}^2 can be computed as

$$\sigma^2_{RES} = \sigma^2_{eQTL}\left(\frac{1}{h^2_{eQTL}} - 1\right)$$

Individual expression data for the corresponding cis-eQTL (for all individuals of the CEDAR dataset) were hence sampled from the normal distribution

$$z_i \sim N(\overline{z_{xx}}, \sigma^2_{RES})$$

where $\overline{z_{xx}}$ is -1, 0 or +1 depending on the genotype of the individual (*11*, *12*, or *22*). We then performed cis-eQTL on the corresponding data set using EAP, generating an in silico EAP. Real and in silico EAP were then compared using ϑ. Supplementary Figure 1 shows the corresponding distribution of ϑ values for EAP driven by distinct regulatory variants.

The corresponding distributions of ϑ under H_1 and H_0 (Supplementary Figure 1) show that ϑ discriminates very effectively between H_1 and H_0 especially for the most significant cis-eQTL. In the experiment described above, this would yield a false positive rate of 0.05, and a false negative rate of 0.23. We chose a threshold of $|\vartheta| > 0.6$ to cluster EAP in cis-acting regulatory elements or cRM (Fig. 2). Clusters were visually examined as show in Supplementary Figure 2. Twenty-nine edges connecting otherwise unlinked and yet tight clusters were manually removed.

Testing for an excess sharing of cRM between cell types

Assume that cell type 1 is part of n_{1T} cRM, including n_{11} private cRM, n_{12} cRM shared with cell type 2, n_{13} cRM shared with cell type 2, …, and n_{19} cRM shared with cell type 9. Note that $\sum_{i=1}^{9} n_{1i} \geq n_{1T}$, because cRM may include more than two cell types. Assume that $n_{1S} = \sum_{i\neq 1}^{9} n_{1i}$ is the sum of pair-wise sharing events for cell type 1. We computed, for each cell type $i \neq 1$, the probability to observe $\geq n_{1i}$ sharing events with cell type 1 assuming that the expected number (under the hypothesis of random assortment) is

$$n_{1S} \times \frac{n_{iT}}{\sum_{j\neq 1}^{9} n_{jT}}$$

Pair-wise sharing events between tissue 1 and the eight other tissues were generated in silico under this model of random assortment (5,000 simulations).

The p-value for n_{1i} was computed as the proportion of simulations that would yield values that would be as large or larger than n_{1i}. The same approach was used for the nine cell types. Thus, two p-values of enrichment are obtained for each pair of cell types *i* and *j*, one using *i* as reference cell type, and the other using *j* as reference cell type. As can be seen from Fig. 5, the corresponding pairs of p-values were always perfectly consistent.

We performed eight distinct analyses. In the first analysis, we only considered cRM involving no more than two tissues (i.e. unique for specific pairs of cell types). In subsequent analyses, we progressively included cRM with no more than three, four, …, and nine cell types.

Comparing EAP and DAP using ϑ

The approach used to cluster EAP in cRM was also used to assign Disease Association Patterns (DAP) for Inflammatory Bowel Disease (IBD) to EAP-defined cRM. We studied 200 IBD risk loci identified in recent GWAS meta-analyses[2,3]. The limits of the corresponding risk loci were as defined in the corresponding publications. We measured the similarity between DAP and EAP using the ϑ metric for all cis-eQTL mapping to the corresponding intervals (i.e. for all cis-eQTL for which the top SNP mapped within the interval). To compute the correlations between DAP and EAP we used all SNPs mapping to the disease interval with –log(p) value ≥ 1.3 either for DAP, EAP or both.

In addition to computing ϑ as described in section 5, we computed an empirical p-value for ϑ using the approach (based on in silico generated cis-eQTL) described above to generate the locus-specific distribution of ϑ values for EAP driven by distinct regulatory variants. From this distribution, one can deduce the probability that a randomly generated EAP (explaining as much variance as the real tested EAP) and the DAP would by chance have a $|\vartheta|$ value that is as high or higher than the real EAP. The corresponding empirical p-value accounts for the local LD structure between SNPs.

Evaluating the enrichment of DAP-EAP matching

To evaluate whether DAP matched EAP more often than expected by chance alone, we analyzed 97 IBD risk loci interrogated by the Immunochip, (i) in order

to allow for convenient comparison with Huang et al.[4], and (ii) because we needed extensively QC genotypes for the IIBDGC data to perform the enrichment analysis with the ϑ-based method (see hereafter). Within these 97 IBD risk loci, we focused on 63 regions affecting CD[4], encompassing at least one significant eQTL, and for which the lead CD-associated SNP had MAF > 0.05. Indeed, eQTL analyses in the CEDAR dataset were restricted to SNPs with MAF > 0.05 (see above). We used three methods to evaluate whether the observed number of DAP-EAP matches were higher than expected by chance alone: naïve, frequentist and ϑ-based. Analyses were performed separately for the nine cell types.

In the "naïve" approach, DAP and EAP were assumed to match if the corresponding lead SNPs were in LD with $r^2 \geq 0.8$. This would yield $n_N \leq 63$ risk loci for which the DAP would match at least one EAP. To measure the statistical significance of n_N, we sampled a SNP (MAF > 0.05) at random in each of the 63 risk loci, and counted the number of loci with at least one matching EAP. This "simulation" was repeated 1,000 times. The significance of n_N was measured as the proportion of simulations that would yield $\geq n_N$ matches.

The frequentist approach used the method described by Nica et al.[53]. DAP and EAP were assumed to match if fitting the disease-associated lead SNP in the eQTL analysis caused a larger drop in $-\log(p)$ than 95% of the SNPs with MAF > 0.05 in the analyzed risk locus. This would yield $n_F \leq 63$ risk loci for which the DAP would match at least one EAP. To measure the statistical significance of n_F, we sampled a SNP (MAF > 0.05) at random in each of the 63 risk loci, and counted the number of loci with at least one matching EAP. This "simulation" was repeated 1,000 times. The significance of n_F was measured as the proportion of simulations that would yield $\geq n_F$ matches.

Finally, we used our ϑ-based approach in which DAP and EAP were assumed to match if $|\vartheta| > 0.6$. This would yield $n_\vartheta \leq 63$ risk loci for which the DAP would match at least one EAP. To measure the statistical significance of n_ϑ we sampled a SNP (MAF > 0.05) at random in each of the 63 risk loci, and generated a DAP assuming that the corresponding SNPs were causal as follows.

Assume a cohort with n_1 cases and n_2 controls (f.i. the IIBDGC cohort). Assume a SNP with an allelic frequency of p in the cases + controls, an allelic frequency of $(p + d)$ in cases and $(p + \delta)$ in controls.

One can easily show that:

$$\delta = -d\frac{n_1}{n_2} \quad (1)$$

The odds ratio (OR) for that SNP equals:

$$OR = \frac{(p + d)(1 - p - \delta)}{(p + \delta)(1 - p - d)}$$

The ratio between the between-cohort (i.e. cases and controls) variance versus within-cohort variance (corresponding to an F test) can be shown to equal:

$$F = \frac{d^2\left(1 + \frac{n_1}{n_2}\right)}{\left(1 + \frac{n_2}{n_1}\right)(p - p^2) - d^2\left(1 + \frac{n_1}{n_2}\right)}$$

If we fix F based on the real top SNP in the IIBDGC data in a given GWAS identified risk loci, we can determine d (and hence δ using equation 1) for the randomly selected SNP (that will become an "in silico causative variant") with allelic frequency in (cases + controls) of p (different from the real top SNP), by solving

$$d = \frac{-\beta \pm \sqrt{\beta^2 - 4\alpha\gamma}}{2\alpha}$$

where

$$\alpha = (1 + \frac{n_1}{n_2})(1 + F)$$

$$\beta = 0$$

$$\gamma = -(p - p^2)\left(1 + \frac{n_2}{n_1}\right)F$$

Once we know $(p + d)$ (i.e. the frequency of the SNP in cases), and hence $(p + \delta)$ (i.e. the frequency of the SNP in controls), we can use Hardy–Weinberg to determine the frequency of the three genotypes in cases $(p_{AA}^{IBD}, p_{AB}^{IBD}, p_{BB}^{IBD})$ and

controls ($p_{AA}^{CTR}, p_{AB}^{CTR}, p_{BB}^{CTR}$). We then create an in silico case-control cohort by sampling (with replacement) $n_1 \times p_{AA}^{IBD}$ AA cases, $n_1 \times p_{AB}^{IBD}$ AB cases, …, and $n_2 \times p_{BB}^{CTR}$ BB controls from the individuals of the IIBDGC (without discriminating real case and control status). Association analysis of the corresponding dataset in the chromosome region of interest generates DAP with $\max - \log(p)$ value similar to the real DAP. This "simulation" was repeated 1,000 times. The significance of n_ϑ was measured as the proportion of simulations that would yield $\geq n_\vartheta$ matches.

Targeted exon resequencing in CD cases and controls

Genes for which EAP match the DAP tightly (high $|\vartheta|$ values) are strong candidate causal genes for the studied disease. In the case of IBD, we identified ~100 such genes (Table 1). Ultimate proof of causality can be obtained by demonstrating a differential burden of rare disruptive variants in cases and controls. Burden tests preferably focus on coding gene segments, in which disruptive variants are most effectively recognized. Analyses are restricted to rare variants to ensure independence from the GWAS signals.

To perform burden tests, we collected DNA samples from 7,323 Crohn Disease (CD) cases and 6,342 controls of European descent in France (cases: 1,899 – ctrls: 1,731), the Netherlands (2,002 – 1,923) and Belgium (3,422 – 2,688). The study protocols were approved by the institutional review board at each centre involved with recruitment. Informed consent and permission to share the data were obtained from all subjects, in compliance with the guidelines specified by the recruiting centre's institutional review board.

During the course of this project, we selected 45 genes with high $|\vartheta|$ values for resequencing (Table 1). We designed primers to amplify all corresponding coding exons plus exon-intron boundaries corresponding to all transcripts reported in the CCDS release 15[54] (Supplemental data 8). Following Momozawa et al.[55], the primers were merged in five pools to perform a first round of PCR amplification (25 cycles). We then added 8-bp barcodes and common adaptors (for sequencing) to all PCR products by performing a second round of PCR amplification (4 cycles) using primers targeting shared 5'overhangs introduced during the first PCR. The ensuing libraries were purified, quality controlled and

sequenced (2 x 150-bp paired-end reads) on a HiSeq 2500 (Illumina) instrument. Sequence reads were sorted by individual using the barcodes, aligned to the human reference sequence (hg19) with the Burrows-Wheeler Aligner (ver. 0.7.12)[56], and further processed using Genome Analysis Toolkit (GATK, ver. 3.2-2)[57]. We only considered individuals for further analyses if ≥ 95% of the target regions was covered ≥ 20 sequence reads. Average sequence depth across individuals and target regions was 1,060. We called variants for each individual separately using the UnifiedGenotyper and HaplotypeCaller of GATK, as well as VCMM (ver. 1.0.2)[58], and listed all variants detected by either method. Genotypes for all individuals were determined for each variant based on the ratio of reference and alternative alleles amongst sequence reads as determined by Samtools[59]. Individuals were labelled homozygote reference, heterozygote, or homozygote derived when the alternative allele frequency was between 0 and 0.15, between 0.25 and 0.75, and between 0.85 and 1, respectively. If the alternative allele frequency was outside these ranges or a variant position was covered with < 20 sequencing reads, the genotype was considered missing. We excluded variants with call rates < 95% or variants that were not in Hardy-Weinberg equilibrium ($P < 1 \times 10^{-6}$). We excluded 281 individuals with ≥ 2 minor alleles at 23 variants selected to have a MAF ≤ 0.01 in non-Finnish Europeans and ≥ 0.10 in Africans or East-Asians in the Exome Aggregation Consortium[60].

In the end, we used 6,597 cases and 5,502 controls for further analyses, while 98.5% of the target regions on average was covered with 20 or more sequence reads.

Gene-based burden test

We first used SIFT[61] and Polyphen-2[62] to sort the 4,175 variants identified by sequencing in four categories: (i) loss-of-function (LoF) or severe, corresponding to stop gain, stop loss, frameshift and splice-site variants, (ii) damaging, corresponding to missense variants predicted by SIFT to be damaging and Polyphen-2 to be possibly or probably damaging, (iii) benign, corresponding to the other missense variants, and (iv) synonymous. We performed the burden test using the LoF plus damaging variants, and used the synonymous variants as controls. We only considered variants with MAF (computed for the entire

dataset, i.e. cases plus controls) ≤ 0.005. We indeed showed in a previous fine-mapping study that all reported independent effects were driven by variants with MAF ≥ 0.01[4]. By doing so we ensure that the signals of the burden test are independent of previously reported association signals. Thus, 174 LoF, 991 damaging, and 1,434 synonymous were ultimately used to perform burden tests.

Burden tests come in two main flavors. In the first, one assumes that disruptive variants will be enriched in either cases (i.e. disruptive variants increase risk) or in controls (i.e. disruptive variance decrease risk). In the second, one assumes that - for a given gene - some disruptive variants will be enriched in cases, while other may be enriched in controls (Supplementary Fig. 11). The first was implemented using CAST[63]. To increase power, we exploited the DAP-EAP information to perform one-sided (rather than two-sided) tests. When $\vartheta < 0$, we tested for an enrichment of disruptive variants in cases; when $\vartheta > 0$, for an enrichment of disruptive variants in controls. P-values were computed by phenotype permutation, i.e. shuffling case-control status. When applying this test on a gene-by-gene basis using synonymous variants (MAF > 0.005), the distribution of p-values (QQ-plot) indicated that the CAST test was conservative ($\lambda_{GC} = 0.51$) (Supplementary Fig. 12). The second kind of burden test was implemented with SKAT[64]. It is noteworthy that SKAT ignores information from singletons (Supplementary Fig. 11). Just as for CAST, p-values were computed by phenotype permutation, i.e. shuffling case-control status. When applying this test on a gene-by-gene basis using synonymous variants (MAF < 0.005), the distribution of p-values (QQ-plot) indicated that the SKAT test is too permissive ($\lambda_{GC} = 1.73$) (Supplementary Fig. 12). Consequently, gene-based p-values obtained with SKAT were systematically GC corrected using this value of λ_{GC}. We performed the two kinds of analyses for each gene, as one doesn't a priori know what hypothesis will match the reality best for a given gene.

We also extracted information from the distribution of p-values (or –log(p) values) across the 45 analyzed genes. Even if individual genes do not yield –log(p) values that exceed the significance threshold (accounting for the number of analyzed genes and tests performed), the distribution of –log(p) values may significantly depart from expectations, indicating that the analyzed genes include at least some causative genes. This was done by taking for each gene, the best p-

value (whether obtained with CAST or SKAT) and then rank the genes by corresponding –log(p) value. The same was done for 10^5 phenotype permutations, allowing us to examine the distribution of –log(p) values for given ranks and compute the corresponding medians and limits of the 95% confidence band, as well as to compute the probability that $-2\sum_{i=1}^{45}\ln(p_i)$ (Fisher's equation to combine p-values) equals or exceeds the observed. Our results show that there is a significant departure from expectation when analyzing the damaging variants ($p = 6.9 \times 10^{-4}$) but not when analyzing the synonymous variants ($p = 0.66$) supporting the presence of genuine causative genes amongst the analyzed list.

cRM-based burden test

The enrichment of multi-genic cRM in IBD risk loci suggests that risk loci may have more than one causative gene belonging to the same cRM. To capitalize on this hypothesis, we developed a cRM-based burden test. Gene-specific p-values were combined within cRM using Fisher's method. For each gene, we considered the best p-value whether obtained with CAST or SKAT. Statistical significance was evaluated by phenotype permutation exactly as described for the gene-based burden test. By doing so we observed a departure from expectation when using the damaging variants ($p = 2.3 \times 10^{-3}$), but not when using the synonymous variants ($p = 0.72$).

Orthogonal tests for age-of-onset and familiality

It is commonly assumed that the heritability for common complex diseases is higher in familial and early onset cases[65]. To extract the corresponding information from our data in a manner that would be orthogonal to the gene- and module-based tests described above (i.e. the information about age-of-onset and familiality would be independent of these burden tests), we devised the following approach.

For age-of-onset, we summed the age-of-onset of the n_C cases carrying rare disruptive variants for the gene of interest. We then computed the probability that the sum of the age-of-onset of n_C randomly chosen cases was as different from the mean of age-of-onset as the observed one, yielding a gene-specific two-

sided p_{SKAT} value. In addition, we used the eQTL information to generate gene-specific one-sided p_{CAST} values, corresponding to the probability that the sum of the age-of-onset of n_C randomly chosen cases was as low or lower than the observed one (for genes for which decrease in expression level as associated with increased risk), or to the probability that the sum of the age-of-onset of n_C randomly chosen cases was as high or higher than the observed one (for genes for which increase in expression level as associated with increased risk). These age-of-onset p-values were then combined with the corresponding p-values from the burden test (CAST with CAST, SKAT with SKAT) using Fisher's method.

For familiality, we determined what fraction of the n_C cases carrying rare disruptive variants for the gene of interest were familial (affected first degree relative). We then computed the probability that the fraction of familial cases amongst n_C randomly chosen cases was as different from the overall proportion of familial cases, yielding a gene-specific two-sided p_{SKAT} value. In addition, we used the eQTL information to generate gene-specific one-sided p_{CAST} values, corresponding to the probability that the fraction of familial cases amongst n_C randomly chosen cases was as high or higher than the observed one (for genes for which decrease in expression level as associated with increased risk), or to the probability that the sum of the age-of-onset of n_C randomly chosen was as low or lower than the observed one (for genes for which increase in expression level as associated with increased risk). These familial p-values were then combined with the corresponding p-values from the burden test (CAST with CAST, SKAT with SKAT) using Fisher's method.

DATA AVAILABILITY

The complete CEDAR eQTL dataset can be downloaded from the Array Express website (https://www.ebi.ac.uk/arrayexpress/), accession numbers E-MTAB-6666 (genotypes) and E-MTAB-6667 (expression data). The data, preprocessed as described in Methods, can be downloaded from the CEDAR website (http://cedar-web.giga.ulg.ac.be).

ACKNOWLEDGEMENTS

This work was supported by grants to Michel Georges from WELBIO (CAUSIBD), BELSPO (BeMGI), and Horizon 2020 (SYSCID). Computational resources at ULg have been provided by GIGA and the Consortium des Équipements de Calcul Intensif (CÉCI), funded by the Fonds de la Recherche Scientifique de Belgique (F.R.S.-FNRS) under Grant No. 2.5020.11. This work was conducted as part of the BioBank Japan Project supported by the Japan Agency for Medical Research and Development and by the Ministry of Education, Culture, Sports, Sciences and Technology of the Japanese government. The work of DA and IA was supported by Russian Ministry of Science and Education under 5-100 Excellence Programme. R.K. Weersma is supported by a VIDI grant (016.136.308) from the Netherlands Organisation for Scientific Research (NWO). DNA samples from the Dutch IBD cohort have been collected within the Parelsnoer Institute Project. This nationwide Parelsnoer Institute project is part of and funded by the Netherlands Federation of University Medical Centres and has received initial funding from the Dutch Government (from 2007-2011). The Parelsnoer Institute currently facilitates the uniform nationwide collection of information on and biomaterials of thirteen other diseases. We are grateful to N. Hakozaki, H. Iijima, N. Maki, and other staff of the Laboratory for Genotyping Development, RIKEN Center for the Integrative Medical Sciences. We thank Wouter Coppieters and the other members of the GIGA genomics platform for their support.

CONFLICTS OF INTEREST

The authors declare absence of any conflict of interest, whether financial or other.

AUTHOR CONTRIBUTIONS

YM, JD and MG conceived experiments, generated data, analyzed data and wrote the manuscript. ET, VD, SR, BC, FC, ED, ME, A-SG,CL,RM,MM,CO generated and analyzed data. IA,DA,YA and MG conceived and generated the CEDAR website. LA, GB, FH, ML, BO, MJP,AEVDMDJ,CJVDW,MVC, ML, JPH, RKW,MDV,DF,SV,MK,EL collected and provided samples.

REFERENCES

1. MacArthur, J. *et al.* The new NHGRI-EBI catalog of published genome-wide association studies (GWAS Catalog). *Nucleic Acids Res* **45**, D896-D901 (2017).
2. Jostins, L. *et al.* Host-microbe interactions have shaped the genetic architecture of inflammatory bowel disease. *Nature* **491**,119-124 (2012).
3. Liu, J.Z. *et al.* Association analyses identify 38 susceptibility loci for IBD and highlight shared genetic risk across populations. *Nat Genet* **47**, 979-986 (2015).
4. Huang, H. *et al.* Association mapping of IBD loci to single variant resolution. *Nature* **547**, 173-178 (2017).
5. Claussnitzer, M. *et al.* FTO obesity variant circuitry and adipocyte browning in humans. *N Engl J Med* **373**, 895-907 (2015).
6. Hugot, J.P. *et al.* Association of NOD2 leucine-rich repeat variants with susceptibility to Crohn's disease. *Nature* **411**, 599-603 (2001).
7. Hampe, J. *et al.* A genome-wide association scan of nonsynonymous SNPs identifies a susceptibility variant for Crohn disease in ATG16L1. *Nat Genet* **39**, 207-211 (2007).
8. Momozawa, Y. *et al.* Resequencing of positional candidates identifies low frequency IL23R coding variants protecting against inflammatory boiwel disease. *Nat Genet* **43**, 43-47 (2011).
9. Rivas, M.A. *et al.* Deep resequencing of GWAS loci identifies independent rare variants associated with inflammatory bowel disease. *Nat Genet* **43**, 1066-1073 (2011).
10. The GTEx Consortium. Genetic effects on gene expression across human tissues. *Nature* **550**, 204-213 (2017).

11. Nica, A.C. *et al.* Candidate causal regulatory effects by integration of expression QTLs with complex trait genetic associations. *PLoS Genet* **6**, e1000895 (2010).
12. Giambartolomei, C. *et al.* Bayesian test for colocalisation between paiurs of genetic association studies using summary statistics. *PLoS Genet* **10**, e1004383 (2014).
13. Zhu, Z. *et al.* Integration of summary data from GWAS and eQTL studies predicts complex trait gene targets. *Nat Genet* **48**, 481-487 (2016).
14. The ENCODE Project Consortium. An integrated encyclopedia of DNA elements in the human genome. *Nature* **489**, 57-74 (2012).
15. Nicolae, D.L. Association tests for rare variants. *Annu Rev Genom Hum Genet* **17**, 117-130 (2016).
16. Pritchard, J.K. & Cox, N.J. The allelic architecture of human disease genes: common disease-common variant … or not? *Hum Mol Genet* **11**, 2417-2423 (2002).
17. McGregor, A.P. *et al.* Morphological evolution through multiple cis-regulatory mutations at a single gene. *Nature* **448**, 587-590 (2007).
18. Mackay, T.F. Quantitative trait loci in Drosophila. *Nat Rev Genet* **2**, 11-20 (2001).
19. Yalcin, B. *et al.* Genetic dissection of behavioral QTL shows that Rgs2 modulates anxiety in mice. *Nat Genet* **36**, 1197-1202 (2004).
20. Karim, L. *et al.* Variants modulating the expression of a chromosome domain encompassing PLAG1 influence bovine stature. *Nat Genet* **43**, 405-413 (2011).
21. Steinmetz, L.M. *et al.* Dissecting the architecture of a QTL in yeast. *Nature* **416**, 326-330 (2002).
22. Khor, B., Gardet, A., Xavier, R. Genetics and pathogenesis of inflammatory bowel disease. *Nature* **474**, 307-317 (2011).
23. https://github.com/joepickrell/1000-genomes-genetic-maps
24. Fuchsberger, C. *et al.* The genetic architecture of type 2 diabetes. *Nature* **536**, 41-47 (2016).
25. Momozawa, Y. *et al.* Low-frequency coding variants in CETP and CFB are associated with susceptibility of exudative age-related macular degeneration in the Japanese population. *Hum. Mol. Genet.* **25**, 5027-5034 (2016).

26. Kumar, P. *et al.* Predicting the effects of coding non-synonymous variants on protein function using gthe SIFT algorithm. *Nat Protoc* **4**, 1073-1081 (2009).
27. Adzhubei, I.A. *et al.* A method and server for predicting damaging missense mutations. *Nat Methods* **7**, 248-249 (2010).
28. Lek, M. *et al.* Analysis of protein-coding genetic variation in 60,706 humans. *Nature* **536**, 285-291 (2016).
29. Morgenthaler, S. & Thilly, W.G. A strategy to discover genes that carry multi-allelic or mono-allelic risk for common diseases: a cohort allelic sums test (CAST). *Mutat Res* **615**, 28–56 (2007).
30. Wu, M.C. *et al.* Rare-variant association testing for sequencing data with the sequence kernel association test. *Am J Hum Genet* **89**, 82-93 (2011).
31. Richardson, T.G. *et al.* A pathway-centric approach to rare variant association analysis. *Eur J Hum Genet* **25**, 123-129 (2017).
32. Imielinski, M. *et al.* Common variants at five new loci associated with early-onset inflammatory bowel disease. *Nat Genet* **41**, 1335-1340 (2009).
33. Chun, S. *et al.* Limited statistical evidence for shared genetic effects of eQTLs and autoimmune-disease-associated loci in three major immune-cell types. *Nat Genet* **4**, 600-605 (2017).
34. The GTEx Consortium. The genotype-tissue expression (GTEx) pilot analysis: multitissue gene regulation in humans. *Science* **348**, 648-660 (2015).
35. Boyle, E.A. *et al.* An expanded view of complex traits: from polygenic to omnigenic. *Cell* **169**, 1177-1186 (2017).
36. Whitehead Pavlides, J.M. *et al.* Predicting targets from integrative analyses of summary data from GWAS and eQTL studies for 28 human complex traits. *Genome Medicine* **8**, 84-90 (2016).
37. Hulur, I. *et al.* Enrichment of inflammatory bowel disease and colorectal cancer risk variants in colon expression quantitative trait loci. *BMC Genomics* **16**, 138-153 (2015).
38. Gamazon, E.R. *et al.* A gene-based association method for mapping traits using reference transcriptome data. *Nat Genet* **47**, 1091-1098 (2015).
39. De Lange, K.M. *et al.* Genome-wide association study implicates immune activation of multiple integrin genes in inflammatory bowel disease. *Nat Genet* **49**, 256-261 (2017).

40. Libioulle, C. *et al.* Novel Crohn disease locus identified by genome-wide association maps to a gene desert on 5p13.1 and modulates expression of PTGER4. *PLoS Genet* **3**, e58 (2007).
41. Peltekova, V.D. *et al.* Functional variants of OCTN cation transporter genes are associated with Crohn disease. *Nat Genet* **39**, 311-318 (2004).
42. McCarroll, S.A. et al. Deletion polymorphism upstream of IRGM expression and Crohn's disease. *Nat Genet* **40**, 1107-112 (2008).
43. https://imputation.sanger.ac.uk
44. The 1000 Genomes Project Consortium. A global reference for human genetic variation. *Nature* **526**, 668-674 (2015).
45. Huang, J. *et al.* Improved imputation of low-frequency and rare variants using the UK10K haplotype reference panel. *Nat Commun* **6**, 8111 (2015).
46. McCarthy *et al.* A reference panel of 64,976 haplotypes for genotype imputation. *Nature Genet.* **48**,1279-1283 (2016).
47. Du, P. *et al.* Lumi: a pipeline for processing illumine microarray. *Bioinformatics* **24**, 1547-1548 (2008).
48. Arloth, J. *et al.* Re-Annotator: annotation pipeline for microarray probe sequences. *PLoS ONE* **10**, e0139516 (2015).
49. Johnson, W.E. *et al.* Adjusting batch effects in microarray expression data using empirical Bayes methods. *Biostatistics* **8**, 118-127 (2007).
50. Fairfax, B.P. et al. Innate immune activity conditions the effect of regulatory variants upon monocyte gene expression. *Science* **343**, 1246949 (2014).
51. http://pngu.mgh.harvard.edu/purcell/plink/
52. Purcell, S. et al. PLINK: a toolset for whole-genome association and population-based linkage analysis. *Am. J. Hum. Genet.* **81**, 559-575(2007).
53. Nica, A.C. *et al.* Candidate causal regulatory effects by integration of expression QTLs with complex trait genetic associations. *PLoS Genet* **6**, e1000895 (2010).
54. Farrell, C.M. *et al.* Current status and new features of the Consensus Coding Sequence database. *Nucleic Acids Res* **42**, D865-72 (2014).
55. Momozawa, Y. *et al.* Low-frequency coding variants in CETP and CFB are associated with susceptibility of exudative age-related macular degeneration in the Japanese population. *Hum. Mol. Genet.* **25**, 5027-5034 (2016).

56. Li, H. & Durbin, R. Fast and accurate short read alignment with Burrows-Wheeler transform. *Bioinformatics* **25**, 1754-60 (2009).
57. Depristo, M.A. *et al.* A framework for variation discovery and genotyping using next-generation DNA sequencing data. *Nat. Genet.* **43**, 491-8 (2011).
58. Shigemizu, D. *et al.* A practical method to detect SNVs and indels from whole genome and exome sequencing data. *Sci Rep* **3**, 2161 (2013).
59. Li, H. *et al.* The sequence alignment/map (SAM) format and SAMtools. *Bioinformatics* **25**,2078-2079 (2009).
60. Lek, M. *et al.* Analysis of protein-coding genetic variation in 60,706 humans. *Nature* **536**, 285-91 (2016).
61. Kumar, P. *et al.* Predicting the effects of coding non-synonymous variants on protein function using gthe SIFT algorithm. *Nat Protoc* **4**, 1073-1081 (2009).
62. Adzhubei, I.A. *et al.* A method and server for predicting damaging missense mutations. *Nat Methods* **7**, 248-249 (2010).
63. Morgenthaler, S. & Thilly, W.G. A strategy to discover genes that carry multi-allelic or mono-allelic risk for common diseases: a cohort allelic sums test (CAST). *Mutat Res 615*, 28–56 (2007).
64. Wu, M.C. *et al.* Rare-variant association testing for sequencing data with the sequence kernel association test. *Am J Hum Genet* **89**, 82-93 (2011).
65. Imielinski, M. *et al.* Common variants at five new loci associated with early-onset inflammatory bowel disease. *Nat Genet* **41**, 1335-1340 (2009).

Figure Legends

Figure 1: cis Regulatory Module (cRM). A cis-eQTL affecting gene A in tissue 1 reveals itself by an "eQTL Association Pattern" ($EAP_{A,1}$), i.e. the pattern of *–log(p)* values for variants in the region. Multiple EAP can be observed in a given chromosome region, affecting one or more genes in one or more cell types. EAP that are driven by the same underlying variants are expected to be similar, while EAP driven by distinct variants (f.i. the green and red regulatory variants in the figure) are not. Based on the measure of similarity introduced in this work, ϑ, we cluster the EAP in cis-Regulatory Modules (cRM). For EAP in the same module, ϑ can be positive or negative, indicating that the variants have the same sign of effect (increasing or decreasing expression) for the corresponding EAP pair.

Figure 2: Single-gene/tissue versus multi-gene/tissue cRM. Using $|\vartheta| > 0.6$, the 23,950 cis-eQTL (FDR ≤ 0.05) detected in the nine analyzed cell types were clustered in 9,691 cis-Regulatory Modules (cRM). 68% of these were single-gene, single-tissue cRM (green), 22% were single-gene, multi-tissue cRM (blue), and 10% were multi-gene, mostly multi-tissue cRM (red). The number of observations for single-gene cRM were divided by 10 in the graph for clarity. Thus, there are more cases of single-gene, multi-tissue cRM (blue; 2,155) than multi-gene cRM (red; 967).

Figure 3: Example of a multi-gene, multi-tissue cRM. Gene-tissue combinations for which no expression could be detected are marked by "-", with detectable expression but without evidence for cis-eQTL as "→", with detectable expression and evidence for a cis-eQTL as "↑" or "↓" (large arrows: FDR < 0.05; small arrows: FDR ≥ 0.05 but high $|\vartheta|$ values). eQTL labelled by the yellow arrows constitute the multi-genic and multi-tissular cRM n°57. The corresponding regulatory variant(s) increase expression of the *GINM1*, *NUP43* and probably *KATNA1* genes (left side of the cRM), while decreasing expression of the *PCMT1* and *LRP11* genes (right side of the cRM). The expression of *GINM1* in CD15 and *LRP11* in CD4 appears to be regulated in opposite directions by a distinct cRM (n°3694, green). The *LATS1* gene, in the same region, is not affected by the same regulatory variants in the studied tissues. Inset 1: ϑ values for all

EAP pairs. EAP pairs with $|\vartheta| > 0.6$ are bordered in yellow when corresponding to cRM n°57, in green when corresponding to cRM n°3694 (+ green arrow).

Figure 4: Variant(s) with opposite effects on expression in two cell types. Example of a gene (*PNKD*) affected by a cis-eQTL in at least two cell types (CD14 and platelets) that are characterized by EAP with ϑ = -0.97, indicating that the gene's expression level is affected by the same regulatory variant in these two cell types, yet with opposite effects, i.e. the variant that is increasing expression in platelets is decreasing expression in CD14.

Figure 5: Significance of the excess sharing of cRM between cell types. (red: p < 0.0002 (Bonferroni corrected 0.0144), orange: p < 0.001 (0.072), rose: p < 0.01 (0.51)). The numbers in the lower-left corner of the squares indicate which cRM were used for the analysis: (2) cRM affecting no more than two cell types, (3) cRM affecting no more than three cell types, etc. The upper-left square indicates the position of the lymphoid cell types (L)(CD4, CD8, CD19), the myeloid cell types (M)(CD14,CD15,PLA), and the intestinal cell types (I)(IL, TR, RE). For each pair of cell types *i* and *j*, we computed two p-values, one using *i* as reference, the other using *j* as reference (Methods). Pairs of p-values were always consistent.

Figure 6: DAP-matching cRM. If a regulatory variant (red) affects disease risk by altering the expression levels of gene B in tissue 2, the $EAP_{B,2}$ is expected to be similar (high $|\vartheta|$) to the "disease association pattern" (DAP), both assigned therefore to the same cRM. ϑ is positive if increased gene expression is associated with increased disease risk, negative otherwise. A cis-eQTL that is driven by a regulatory variant (green) that does not directly affect disease risk, will be characterized by an EAP (say gene A, tissue 2, $EAP_{A,2}$) that is not similar to the DAP (low $|\vartheta|$).

Figure 7: Screen shots of the CEDAR website, showing (i) known CD risk loci on the human karyotype, (ii) a zoom in the HD35 risk locus showing the Refseq gene content and summarizing local CEDAR cis-eQTL data (white: no expression data, gray: expression data but no evidence for cis-e, black: significant cis-eQTL but no correlation with DAP, red: significant cis-eQTL similar to DAP ($\vartheta \leq -0.75$), green: significant cis-eQTL similar to DAP ($\vartheta \geq 0.75$)), and (iii) a zoom in

the DAP for Crohn's disease (black) and EAP for *IL18R1* (red), as well as the signed correlation between DAP and EAP.

Figure 8: Variants detected by sequencing the coding exons of 45 candidate genes. Variants are sorted in LoF (Loss-of-Function, i.e. stop gain, frame-shift, splice site), Damaging MS (missense variants considered as damaging by SIFT[5] and damaging or possibly damaging by Polyphen-2[6]), Benign MS (other missense variants), and Synonymous. Blue: variants with MAF < 0.005, Red: variants with MAF $\geq$ 0.005.

Figure 9: QQ-plot for the gene-based burden test. Ranked log(1/p) values obtained when considering LoF and damaging variants (full circles), or synonymous variants (empty circles). The circles are labeled in blue when the best p-value for that gene is obtained with CAST, in red when the best p-value is obtained with SKAT. The black line corresponds to the median log(1/p) value obtained (for the corresponding rank) using the same approach on permuted data (LoF and damaging variants). The grey line marks the upper limit of the 95% confidence band. The name of the genes with nominal p-value $\leq$ 0.05 are given. Known causative genes are italicized. The inset p-value corresponds to the significance of the upwards shift in log(1/p) values estimated by permutation.

1153

Table 1

Loc	Chr	Beg	End	cRM	Nr	Genes with correlated DAP-EAP	Implicated cell types	Best theta		Best p		Ref
								CD	UC	CD	UC	
HD1	1	2.4	2.8	271	2	*TNFRSF14*	CD4 CD8 IL TR	-0.74	-0.79	0.02	0.03	4 36
HD2	1	7.7	8.3	2900	1	PARK7	CD15 TR RE	-0.8	-0.82	0.01	0.06	36
N_1_62	1	62.5	63.5	109	3	**DOCK7** USP1 ATG4C	CD4 CD8 **CD19** CD14 CD15	-0.9	0	0.01	1.00	3
N_1_100	1	101.0	102.0	6008	1	SLC30A7	TR	0	-0.71	1.00	0.06	
J_1_119	1	120.2	120.7	9459	1	NOTCH2	CD19	0.68	0	0.13	1.00	
HD14	1	155.0	156.1	5	8	GBA	CD4	-0.65	0	0.01	1.00	
				238	3	*THBS3* GBA MUC1	CD14 CD15 TR	0	0.81	1.00	0.02	
				4513	1	*THBS3*	CD4	0	0.66	1.00	0.02	
HD21	1	197.3	198.0	6071	1	DENND1B	CD4	0.7	0.78	0.03	0.02	
HD30	2	62.4	62.7	3716	1	B3GNT2	CD8	-0.63	0	0.01	1.00	
HD35	2	102.8	103.3	1132	1	***IL18R1***	**CD4 CD8**	-0.93	-0.87	0.01	0.03	4
				8912	1	(IL18RAP)	CD8	-0.42	0	0.11	0.38	4
J_2_197	2	198.2	199.1	325	2	MARS2 *PLCL1*	CD4 CD14	-0.72	0	0.06	1.00	2 36
J_2_218	2	218.9	219.4	216	3	PNKD GPBAR1	CD14 TR RE	0.72	0.72	0.01	0.06	2 36
HD43	2	234.1	234.6	1177	1	***ATG16L1***	CD4 CD8 IL TR RE	0.94	0	0.05	1.00	2 39
N_3_45	3	46.0	47.0	2930	1	CCR2	CD19	0.77	0	0.02	1.00	
				1203	1	CCR2	CD4	-0.62	0	0.07	1.00	
				7768	1	CCR9	CD19	0	-0.67	1.00	0.06	
				6798	1	KLHL18	CD14	0	-0.68	1.00	0.03	
				8	7	*USP4*	CD19	0.64	0.63	0.06	0.07	2
HD50	3	48.4	51.4	217	3	***GPX1 APEH*** *IP6K1*	**CD19** CD14 **TR RE**	0.91	0.97	0.01	0.01	2 39
				122	3	*FAM212A*	CD19	0	0.61	1.00	0.05	
J_3_52	3	52.8	53.3	3190	1	SFMBT1	TR RE	0	-0.88	1.00	0.01	37
J_4_73	4	74.6	75.1	1271	1	CXCL5	CD4 CD8 CD19 CD14 PLA	0	-0.84	1.00	0.01	2
HD60	5	40.0	40.7			(*PTGER4*)	CD15	0	0	0.28	0.15	40
HD61	5	55.4	55.5	360	2	***ANKRD55*** **IL6ST**	**CD4** CD8	0.9	0	0.02	1.00	4
HD62	5	72.4	72.6	6625	1	FOXD1	IL	-0.74	0	0.03	1.00	4
HD63	5	95.9	96.5	365	2	***ERAP2*** *LNPEP*	**CD4 CD8 CD19 CD14 CD15** PLA **IL TR RE**	0.94	0.71	0.01	0.02	2 4 37
HD65	5	130.4	132.0	55	4	(*SLC22A4*) (*SLC22A5*)	CD4 CD15	-0.55	0	0.06	0.07	4 41
HD66	5	141.4	141.7	2389	1	*NDFIP1*	CD8 PLA	0.87	0.88	0.04	0.01	2
HD67	5	149.0	151.0	-	-	(*IRGM*)	-	-	-	-	-	42
HD71	5	173.2	173.6	1349	1	*CPEB4*	**CD4** CD8 CD19 **CD14** CD15 PLA TR	-0.92	0	0.01	1.00	2 4
J_66_32	6	32.3	32.9	7853	1	HLA-DQA2	IL	0	-0.62	1.00	0.02	
HD76	6	90.8	91.1	1404	1	BACH2	CD4	0.67	0	0.14	1.00	
HD78	6	111.3	112.0	9603	1	SLC16A10	IL	0	-0.71	1.00	0.11	
HD80	6	127.9	128.4	707	2	**THEMIS** PTPRK	**CD8**	-0.92	0	0.01	1.00	
HD83	6	167.3	167.6	1425	1	*RNASET2*	CD4 CD8 CD15 PLA	-0.87	0	0.02	1.00	4
J_7_1	7	2.5	3.0	2729	1	**GNA12**	**CD19** CD14 TR	0	-0.94	1.00	0.02	2
HD84	7	26.6	27.3	1441	1	***SKAP2***	**CD4 CD8 CD19**	0.97	0	0.01	1.00	4
HD85	7	28.1	28.3	6438	1	*JAZF1*	CD4	0.78	0	0.01	1.00	2
HD92	7	128.5	128.8	401	2	IRF5 *TNPO3*	CD15 IL	0	-0.64	1.00	0.02	2 36
				7046	1	TSPAN33	CD19	-0.64	0	0.01	1.00	
N_8_26	8	26.7	27.7	5869	1	PTK2B	CD14	-0.69	0	0.01	1.00	
				5841	1	TRIM35	CD4	0	0.66	1.00	0.01	
HD106	9	139.1	139.5	64	4	***CARD9*** INPP5E *SEC16A SDCCAG3*	CD4 CD8 CD19 CD14 **CD15** IL TR RE	0.95	0.86	0.01	0.02	2 4 37
HD109	10	30.6	30.9	1603	1	MTPAP	TR	-0.62	0	0.11	1.00	
HD112	10	59.8	60.2	1609	1	***CISD1***	**CD4 CD8 CD19 CD14 CD15 TR** RE	0.94	0.83	0.04	0?01	2 4 36
J_10_74	10	75.4	75.9	436	2	*VCL*	CD4 CD8 CD19 CD14 RE	0	-0.79	1.00	0.04	
				4279	1	CAM2KG	CD4	-0.67	0	0.04	1.00	
HD114	10	81.0	81.2	5476	1	**ZMIZ1**	**CD8**	-0.91	-0.86	0.03	0.01	
J_10_80	10	82.0	82.5	712	2	TSPAN14	TR	-0.71	0	0.01	1.00	
				2216	1	TSPAN14	CD4 CD14	0.76	0	0.01	1.00	2
HD116	10	101.2	101.4	5439	1	*SLC25A28*	CD14	-0.61	0	0.22	1.00	
J_11_57	11	58.1	58.6	7164	1	ZFP91	PLA	-0.64	-0.75	0.02	0.07	
J_11_59	11	61.3	61.8	1670	1	TMEM258	CD4 CD8 CD19	0.83	0	0.04	1.00	
J_11_65	11	65.4	65.9	451	2	CTSW FIBP	CD4 CD8	-0.73	0	0.01	1.00	2
HD122	11	114.2	114.6	268	3	REXO2 NXPE1 NXPE4	TR RE	0	-0.89	1.00	0.02	4 37
HD123	11	118.3	118.8	8200	1	TREH	IL	0	0.7	1.00	0.05	
HD142	14	88.2	88.7	8940	1	GPR65	CD14	0.8	0.79	0.01	0.01	
				6353	1	(*GALC*)	CD14	-0.52	-0.23	0.06	0.06	4
J_15_40	15	41.3	41.8	9109	1	CHP1	IL	0.62	0	0.01	1.00	
J_16_22	16	23.6	24.1	2672	1	PRKCB	CD14	0	0.64	1.00	0.05	2
HD150	16	28.2	29.1	6	8	*TUFM* SBK1 APOBR *SGF29 CLN3 SPNS1*	CD4 CD8 CD19 CD14 CD15 IL TR RE	0.81	0.86	0.05	0.03	4
HD151	16	30.4	31.4	2673	1	RNF40	CD15	-0.63	0	0.02	1.00	
				1886	1	*ITGAL*	CD4 CD8 CD19	0	0.74	1.00	0.01	39
HD153	16	68.4	68.9	1894	1	ZFP90	CD4 CD8 CD19 CD14 TR	0	0.83	1.00	0.07	2 36
HD156	16	85.9	86.1	3328	1	*IRF8*	TR RE	0	0.72	1.00	0.01	
HD159	17	37.3	38.3	37	5	***GSDMB ORMDL3*** *PGAP3 (GSDMA)*	**CD4 CD8 CD19** CD14 **IL TR RE**	-0.98	-0.92	0.02	0.01	2 4
HD161	17	40.3	41.0	836	2	*STAT3*	PLA	0.67	0	0.10	1.00	
HD164	18	67.4	67.6	1988	1	CD226	CD4 CD8 PLA	0	-0.86	1.00	0.01	2
N_18_76	18	76.7	77.7	7292	1	PQLC1	PLA	-0.68	0	0.01	1.00	
HD166	19	10.3	10.7	9232	1	(*TYK2*)	CD14	-0.44	-0.09	0.10	0.10	
HD168	19	47.1	47.4	581	2	GNG8	CD4	0	-0.63	1.00	0.06	
HD169	19	49.0	49.3	3128	1	***FUT2***	**IL TR RE**	-0.95	0	0.01	1.00	4
J_20_31	20	31.1	31.6	593	2	COMMD7	CD14	0	0.61	1.00	0.01	
J_20_32	20	33.6	34.1	7	8	UQCC1	CD19	-0.69	0	0.02	1.00	2
				3369	1	MMP24-AS1	RE	-0.63	-0.71	0.03	0.03	
HD175	20	62.2	62.5	2322	1	*LIME1*	CD4 CD19	-0.86	0	0.01	1.00	2
HD176	21	16.6	16.9	9578	1	NRIP1	CD4	0	-0.69	1.00	0.02	
HD180	22	21.7	22.1	2130	1	**UBE2L3**	**CD4 CD8 CD19 CD14 CD15 IL TR RE**	0.97	0.92	0.01	0.07	2 4
N_22_41	22	41.4	42.4	2149	1	EP300	CD8 CD19 CD15	0	0.71	1.00	0.02	

1154

Table 1: IBD risk loci for which at least one cis-eQTL association pattern (EAP) was found to match the disease association pattern (DAP). Given are (i) the name and chromosomal coordinates of the corresponding loci (Locus, Chr, Beg, End)(GRCh37/hg19 in Mb), (ii) the identifier and total number of genes in the matching cis-acting regulatory module (cRM, Nr), (iii) the genes and tissues involved in matching DAP-EAP ($|\vartheta| > 0.6$) (bold when $|\vartheta| \geq 0.9$), (iv) the best ϑ-values and corresponding empirical p-values obtained for CD and UC, respectively, and (vi) references reporting a link between one or more of the same genes and IBD on the basis of eQTL information. Genes that were resequenced are shown in italics. Genes that were resequenced despite $|\vartheta| \leq 0.6$ are bracketed, and the supporting references provided in "Ref". The higher number of matching DAP-EAP in this study when compared to Huang et al. [4] are primarily due to the fact that (i) we herein study 200 IBD risk loci (vs 97), and (ii) we increase the number of detected cis-eQTL approximately two-fold by correcting for hidden confounders using PCs.

The International IBD Genetics Consortium

Clara Abraham[23], Jean-Paul Achkar[24,25], Tariq Ahmad[26], Ashwin N Ananthakrishnan[27,28], Vibeke Andersen[29,30,31], Carl A Anderson[32], Jane M Andrews[33], Vito Annese[34,35], Guy Aumais[36,37], Leonard Baidoo[38], Robert N Baldassano[39], Peter A Bampton[40], Murray Barclay[41], Jeffrey C Barrett[32], Theodore M Bayless[42], Johannes Bethge[43], Alain Bitton[44], Gabrielle Boucher[45], Stephan Brand[46], Berenice Brandt[43], Steven R Brant[42], Carsten Büning[47], Angela Chew[48,49], Judy H Cho[50], Isabelle Cleynen[21], Ariella Cohain[51], Anthony Croft[52], Mark J Daly[53,54], Mauro D'Amato[55,56,57], Silvio Danese[58], Dirk De Jong[11], Goda Denapiene[59], Lee A Denson[60], Kathy L Devaney[27], Olivier Dewit[61], Renata D'Inca[62], Marla Dubinsky[63], Richard H Duerr[38,64], Cathryn Edwards[65], David Ellinghaus[66], Jonah Essers[67,68], Lynnette R Ferguson[69], Eleonora A Festen[17], Philip Fleshner[70], Tim Florin[71], Andre Franke[66], Karin Fransen[72], Richard Gearry[41,73], Christian Gieger[74], Jürgen Glas[46,75], Philippe Goyette[45], Todd Green[54,67], Anne M Griffiths[76], Stephen L Guthery[77], Hakon Hakonarson[78], Jonas Halfvarson[78], Katherine Hanigan[52], Talin Haritunians[70], Ailsa Hart[79], Chris Hawkey[80], Nicholas K Hayward[81], Matija Hedl[23], Paul Henderson[82,83], Xinli Hu[84], Hailiang Huang[53,54], Ken Y Hui[50], Marcin Imielinski[39], Andrew Ippoliti[70], Laimas Jonaitis[85], Luke Jostins[86,87], Tom H Karlsen[88,89,90], Nicholas A Kennedy[91], Mohammed Azam Khan[92,93], Gediminas Kiudelis[85], Krupa Krishnaprasad[94], Subra Kugathasan[95], Limas Kupcinskas[96], Anna Latiano[34], Debby Laukens[20], Ian C Lawrance[48,97], James C Lee[98], Charlie W Lees[91], Marcis Leja[99], Johan Van Limbergen[76], Paolo Lionetti[100], Jimmy Z Liu[32], Gillian Mahy[101], John Mansfield[102], Dunecan Massey[98], Christopher G Mathew[103,104], Dermot PB McGovern[70], Raquel Milgrom[105], Mitja Mitrovic[72,106], Grant W Montgomery[81], Craig Mowat[107], William Newman[92,93], Aylwin Ng [27,108], Siew C Ng[109], Sok Meng Evelyn Ng[23], Susanna Nikolaus[43], Kaida Ning[23], Markus Nöthen[110], Ioannis Oikonomou[23], Orazio Palmieri[34], Miles Parkes[98], Anne Phillips[107], Cyriel Y Ponsioen[12], Urõs Potocnik[106,111], Natalie J Prescott[103], Deborah D Proctor[23], Graham Radford-Smith[52,112], Jean-Francois Rahier[113], Soumya Raychaudhuri[84], Miguel Regueiro[38], Florian Rieder[24], John D Rioux[36,45], Stephan Ripke[53,54], Rebecca Roberts[41], Richard K Russell[82], Jeremy D Sanderson[114], Miquel Sans[115], Jack Satsangi[91], Eric E Schadt[51], Stefan Schreiber[43,66], Dominik Schulte[43], L Philip Schumm[116], Regan Scott[38], Mark Seielstad[117,118], Yashoda Sharma[23], Mark S Silverberg[105], Lisa A Simms[52], Jurgita Skieceviciene[85], Sarah L Spain[32,119], A. Hillary Steinhart[105], Joanne M Stempak[105], Laura Stronati[120], Jurgita Sventoraityte[94], Stephan R Targan[70], Kirstin M Taylor[114], Anje ter Velde[12], Leif Torkvist[121], Mark Tremelling[122], Suzanne van Sommeren[17], Eric Vasiliauskas[70], Hein W Verspaget[15], Thomas Walters[76,123], Kai Wang[39], Ming-Hsi Wang [24,42], Zhi Wei[124], David Whiteman[81], Cisca Wijmenga[72], David C Wilson[82,83], Juliane Winkelmann[125,1266], Ramnik J Xavier[27,54], Bin Zhang[51], Clarence K Zhang[127], Hu Zhang[128,129], Wei Zhang[23], Hongyu Zhao[127], Zhen Z Zhao[81]

[23]Section of Digestive Diseases, Department of Internal Medicine, Yale School of Medicine, New Haven, Connecticut, USA. [24]Department of Gastroenterology and Hepatology, Digestive Disease Institute, Cleveland Clinic, Cleveland, Ohio, USA. [25]Department of Pathobiology, Lerner Research Institute, Cleveland Clinic, Cleveland, Ohio, USA. [26]Peninsula College of Medicine and Dentistry,

Exeter, UK. [27]Gastroenterology Unit, Massachusetts General Hospital, Harvard Medical School, Boston, Massachusetts 02114, USA. [28]Division of Medical Sciences, Harvard Medical School, Boston, Massachusetts, USA. [29]Focused research unit for Molecular Diagnostic and Clinical Research (MOK), IRS-Center Sonderjylland, Hospital of Southern Jutland, 6200 Åbenrå, Denmark. [30]Institute of Molecular Medicine, University of Southern Denmark, 5000 Odense, Denmark. [31]Institute of Regional Health Research , University of Southern Denmark, Odense, Denmark. [32]Wellcome Trust Sanger Institute, Wellcome Genome Campus, Hinxton, Cambridgeshire CB10 1SA, UK. [33]Inflammatory Bowel Disease Service, Department of Gastroenterology and Hepatology, Royal Adelaide Hospital, Adelaide, Australia. [34]Unit of Gastroenterology, Istituto di Ricovero e Cura a Carattere Scientifico-Casa Sollievo della Sofferenza (IRCCS-CSS) Hospital, San Giovanni Rotondo, Italy. [35]Strutture Organizzative Dipartimentali (SOD) Gastroenterologia 2, Azienda Ospedaliero Universitaria (AOU) Careggi, Florence, Italy. [36]Facult de Médecine, Universit de Montréal, Montréal, Québec H3C 3J7, Canada. [37]Department of Gastroenterology, Hôpital Maisonneuve-Rosemont, Montréal, Québec, Canada. [38]Division of Gastroenterology, Hepatology and Nutrition, Department of Medicine, University of Pittsburgh School of Medicine, Pittsburgh, Pennsylvania 15213, USA. [39]Center for Applied Genomics, The Children's Hospital of Philadelphia, Philadelphia, Pennsylvania, USA. [40]Department of Gastroenterology and Hepatology, Flinders Medical Centre and School of Medicine, Flinders University, Adelaide, Australia. [41]Department of Medicine, University of Otago, Christchurch, New Zealand. [42]Meyerhoff Inflammatory Bowel Disease Center, Department of medicine, Johns Hopkins University School of Medicine, Baltimore, Maryland, USA. [43]Department for General Internal Medicine, Christian-Albrechts-University, Kiel, Germany. [44]Division of Gastroenterology, Royal Victoria Hospital, Montréal, Québec, Canada. [45]Research Center, Montreal Heart Institute, Montréal, Québec H1T 1C8, Canada. [46]Department of Medicine II, Ludwig-Maximilians-University Hospital Munich-Grosshadern, Munich, Germany. [47]Department of Gastroenterology, Campus Charité Mitte, Universitatsmedizin Berlin, Berlin, Germany. [48]Harry Perkins Institute for Medical Research, School of Medicine and Pharmacology, University of Western Australia, Murdoch, Western Australia 6150, Australia. [49]IBD unit , Fremantle Hospital, Fremantle, Australia. [50]Department of Genetics, Yale School of Medicine, New Haven, Connecticut 06510, USA. [51]Department of Genetics and Genomic Sciences, Mount Sinai School of Medicine, New York, New York, USA. [52]Inflammatory Bowel Diseases, Genetics and Computational Biology, Queensland Institute of Medical Research, Brisbane, Australia. [53]Analytic and Translational Genetics Unit, Massachusetts General Hospital, Harvard Medical School, Boston, Massachusetts 02114, USA. [54]Broad Institute of MIT and Harvard, Cambridge, Massachusetts 02141, USA. [55]Clinical Epidemiology Unit, Department of Medicine Solna, Karolinska Institutet, 17176 Stockholm, Sweden. [56]Department of Gastrointestinal and Liver Diseases, BioDonostia Health Research Institute, 20014 San Sebastián, Spain. [57]IKERBASQUE, Basque Foundation for Science, 48013 Bilbao, Spain. [58]IBD Center, Department of Gastroenterology, Istituto Clinico Humanitas, Milan, Italy. [59]Center of hepatology, Gastroenterology and Dietetics, Vilnius University, Vilnius, Lithuania. [60]Pediatric

Gastroenterology, Cincinnati Children's Hospital Medical Center, Cincinnati, Ohio, USA. [61]Department of Gastroenterology, Université Catholique de Louvain (UCL) Cliniques Universitaires Saint-Luc, Brussels, Belgium. [62]Division of Gastroenterology, University Hospital Padua, Padua, Italy. [63]Department of Pediatrics, Cedars Sinai Medical Center, Los Angeles, California, USA. [64]Department of Human Genetics, University of Pittsburgh Graduate School of Public Health, Pittsburgh, Pennsylvania 15261, USA. [65]Department of Gastroenterology, Torbay Hospital, Torbay, Devon, UK. [66]Institute of Clinical Molecular Biology, Christian-Albrechts-University of Kiel, 24118 Kiel, Germany. [67]Center for Human Genetic Research, Massachusetts General Hospital, Harvard Medical School, Boston, Massachusetts, USA. [68]Pediatrics, Harvard Medical School, Boston, Massachusetts, USA. [69]Faculty of Medical & Health Sciences, School of Medical Sciences, The University of Auckland, Auckland, New Zealand. [70]F. Widjaja Foundation Inflammatory Bowel and Immunobiology Research Institute, Cedars-Sinai Medical Center, Los Angeles, California 90048, USA. [71]Department of Gastroenterology, Mater Health Services, Brisbane, Australia. [72]Department of Genetics, University Medical Center Groningen, Groningen, The Netherlands. [73]Department of Gastroenterology, Christchurch Hospital, Christchurch, New Zealand. [74]Institute of Genetic Epidemiology, Helmholtz Zentrum München - German Research Center for Environmental Health, Neuherberg, Germany. [75]Department of Preventive Dentistry and Periodontology, Ludwig-Maximilians-University Hospital Munich-Grosshadern, Munich, Germany. [76]Division of Pediatric Gastroenterology, Hepatology and Nutrition, Hospital for Sick Children, Toronto, Ontario, Canada. [77]Department of Pediatrics, University of Utah School of Medicine, Salt Lake City, Utah, USA. [78]Department of Gastroenterology, Faculty of Medicine and Health, Örebro University, SE-70182 Örebro, Sweden. [79]Department of Medicine, St Mark's Hospital, Harrow, Middlesex, UK. [80]Nottingham Digestive Diseases Centre, Queens Medical Centre, Nottingham, UK. [81]Molecular Epidemiology, Genetics and Computational Biology, Queensland Institute of Medical Research, Brisbane, Australia. [82]Paediatric Gastroenterology and Nutrition, Royal Hospital for Sick Children, Edinburgh, UK. [83]Child Life and Health, University of Edinburgh, Edinburgh, Scotland, UK. [84]Division of Rheumatology Immunology and Allergy, Brigham and Women's Hospital, Boston, Massachusetts, USA. [85]Academy of Medicine, Lithuanian University of Health Sciences, Kaunas, Lithuania. [86]Wellcome Trust Centre for Human Genetics, University of Oxford, Headington OX3 7BN, UK. [87]Christ Church, University of Oxford, St Aldates OX1 1DP, UK. [88]Research Institute of Internal Medicine, Department of Transplantation Medicine, Division of Cancer, Surgery and Transplantation, Oslo University Hospital Rikshospitalet, Oslo, Norway. [89]Norwegian PSC Research Center, Department of Transplantation Medicine, Division of Cancer, Surgery and Transplantation, Oslo University Hospital Rikshospitalet, Oslo, Norway. [90]K.G. Jebsen Inflammation Research Centre, Institute of Clinical Medicine, University of Oslo, Oslo, Norway.[91]Gastrointestinal Unit, Western General Hospital University of Edinburgh, Edinburgh, UK.

[92]Genetic Medicine, Manchester Academic Health Science Centre, Manchester, UK. [93]The Manchester Centre for Genomic Medicine, University of Manchester, Manchester, UK. [94]QIMR Berghofer Medical Research Institute, Royal Brisbane Hospital, Brisbane, Australia. [95]Department

of Pediatrics, Emory University School of Medicine, Atlanta, Georgia, USA. [96]Department of Gastroenterology, Kaunas University of Medicine, Kaunas, Lithuania. [97]Centre for Inflammatory Bowel Diseases, Saint John of God Hospital, Subiaco, Western Australia 6008, Australia. [98]Inflammatory Bowel Disease Research Group, Addenbrooke's Hospital, Cambridge CB2 0QQ, UK. [99]Faculty of medicine, University of Latvia, Riga, Latvia. [100]Dipartimento di Neuroscienze, Psicologia, Area del Farmaco e Salute del Bambino, Universitˆ di Firenze Strutture Organizzative Dipartimentali (SOD) Gastroenterologia e Nutrizione Ospedale pediatrico Meyer, Firenze, Italy. [101]Department of Gastroenterology, The Townsville Hospital, Townsville, Australia.

[102]Institute of Human Genetics, Newcastle University, Newcastle upon Tyne, UK. [103]Department of Medical and Molecular Genetics, King's College London, London SE1 9RT, UK. [104]Sydney Brenner Institute for Molecular Bioscience, University of the Witwatersrand, Johannesburg 2193, South Africa. [105]Inflammatory Bowel Disease Centre, Mount Sinai Hospital, Toronto, Ontario, Canada. [106]Center for Human Molecular Genetics and Pharmacogenomics, Faculty of Medicine, University of Maribor, Maribor, Slovenia. [107]Department of Medicine, Ninewells Hospital and Medical School, Dundee, UK. [108]Center for Computational and Integrative Biology, Massachusetts General Hospital, Harvard Medical School, Boston, Massachusetts, USA. [109]Department of Medicine and Therapeutics, Institute of Digestive Disease, Chinese University of Hong Kong, Hong Kong. [110]Department of Genomics Life & Brain Center, University Hospital Bonn, Bonn, Germany. [111]Faculty for Chemistry and Chemical Engineering, University of Maribor, Maribor, Slovenia. [112]Department of Gastroenterology, Royal Brisbane and Womens Hospital, Brisbane, Australia. [113]Department of Gastroenterology, Université Catholique de Louvain (UCL) Centre Hospitalier Universitaire (CHU) Mont-Godinne, Mont-Godinne, Belgium. [114]Department of Gastroenterology, Guy's & St Thomas' NHS Foundation Trust, St-Thomas Hospital, London, UK. [115]Department of Digestive Diseases, Hospital Quiron Teknon, Barcelona, Spain. [116]Department of Public Health Sciences, University of Chicago, Chicago, Illinois, USA. [117]Human Genetics, Genome Institute of Singapore, Singapore. [118]Institute for Human Genetics, University of California, San Francisco, San Francisco, California, USA. [119]Open Targets, Wellcome Trust Genome Campus, Hinxton, Cambridgeshire CB10 1SD, UK. [120]Department of Biology of Radiations and Human Health, Agenzia nazionale per le nuove tecnologie l'energia e lo sviluppo economico sostenibile (ENEA), Rome, Italy. [121]Department of Clinical Science Intervention and Technology, Karolinska Institutet, Stockholm, Sweden. [122]Gastroenterology & General Medicine, Norfolk and Norwich University Hospital, Norwich, UK. [123]Faculty of medicine, University of Toronto, Toronto, Ontario, Canada. [124]Department of Computer Science, New Jersey Institute of Technology, Newark, New Jersey, USA. [125]Institute of Human Genetics, Technische Universität München, Munich, Germany.[126]Department of Neurology, Technische Universität München, Munich, Germany. [127]Department of Biostatistics, School of Public Health, Yale University, New Haven, Connecticut, USA. [128]Department of Gastroenterology, West China Hospital, Chengdu, Sichuan, China. [129]State Key Laboratory of Biotherapy, Sichuan University West China University of Medical Sciences (WCUMS), Chengdu, Sichuan, China.

1333

Supplementary Information

IBD risk loci are enriched in multigenic regulatory modules encompassing causative genes.

Momozawa et al.

Supplementary note 1: Genes with strong DAP-EAP correlation

IL18R1 encodes the IL-18r1, the receptor of IL-18, a potent proinflammatory cytokine governing host-microorganism homeostasis and is postulated to play a role in IBD[1,2]. However, IL-18/IL-18r1 precise contribution to the disease remains controversial. Indeed, compared to wild-type mice, *Il18*$^{-/-}$ and *Il18r1*$^{-/-}$ full KO mice are more susceptible to AOM/DSS-induced colitis and polyp formation[3]. However, targeted deletion of *Il18*$^{-/-}$ and *Il18r1*$^{-/-}$ in intestinal epithelial cells confers protection from colitis and mucosal damage in mice[4]. In human, several studies have associated circulating or local IL-18 with IBD severity, suggesting that IL-18 could be an effector cytokine in IBD[5].

IL6ST encodes the interleukin 6 signal transducer protein (IL6ST), also called IL6 beta, GP130 or CD130. IL6ST is a common transmenbrane receptor for all family members of IL6 that include IL-6, IL-11, ciliary neurotrophic factor (CNTF), cardiotrophin-1 (CT-1), cardiotrophin like cytokine (CLC), leukaemia inhibitory factor (LIF), oncostatin M (OSM), neuropoitin (NPN) and interleukin-27 (IL-27)[6]. IL6 family members / IL6ST signaling pathways involve the activation of JAK (Janus kinase) family members, leading to the activation of STAT (signal transducers and activators of transcription) family, as well as the activation of MAPK (mitogen-activated protein kinase) pathway. These pathways are involved in cell survival, apoptosis, differentiation and proliferation[6]. The involvement of IL6/IL6ST/STAT3 in the pathophysiology of IBD is well documented[7]. Indeed, high circulating levels of IL6 is associated with increased severity of the disease[7]. T cells from IBD patient show increased STAT3 activation with increased expression of IL6ST and enhanced resistance to apoptosis[8]. A pilot clinical trial (phase I) targeting of IL6/IL6ST pathway in patients with CD has shown that blocking this pathway has effects similar to the inhibition of TNF[9,10].

THEMIS encodes the thymocyte-expressed molecule involved in selection (THEMIS), the expression of which is limited to lymphoid tissues. In mice, THEMIS is highly expressed in pre-TcR thymocytes and plays an important role in T-cell development and TCR activation signaling[11,12]. Its expression is reduced in differentiated T lymphocytes[12]. THEMIS deficiency in mice is associated with the

presence of higher percent of T_{reg} cells, with reduced TCR-mediated T cell response, increased proportion of memory CD4 and CD8 T cells and reduced proportions of naïve-phenotype populations[12]. Interestingly, all these T cells associated feathers are implicated in the pathogenesis of IBD. Indeed, lamina propria T cells in IBD are hypo-responsive to TCR stimulation and high number of effector T cells are present in the inflamed bowel[13]. As for T_{reg}, only moderate expansion was seen in intestinal lesions of Crohn's patients suggesting that their suppressive activity is probably not sufficient against the overwhelming effector T cells activity[13].

APEH encodes the acylpeptide hydrolase (APEH) enzyme that contributes to protein degradation processes in concert with the proteasome. It catalyzes the removal of *N*-acylated amino acids from acetylated peptides[14]. Its physiological role is not well undertood. SNPs in APEH gene hves been associated with both CD and UC[15]. Like other ubiquitin proteasome systems (UPS) such as USP40 or CYLD, APEH may also regulate the NF-kB pathway. Under this scenario, an alteration of NF-kB signaling may lead to aberrant immune response and inflammation.

ANKRD55 encodes an Ankyrin repeat domain-containing protein 55 with unknown function. Ankyrin repeats are composed of 33-34 aa and are the most abundant motifs in nature with highly diverse cellular functions[16]. SNPs at the ANKRD55 locus have also been associated with multiple sclerosis[17] and RA[18].

CISD1 gene encodes a highly conserved iron-sulfur domain-containing protein A, known as mitoNEET. This iron-containing protein is a dynamic redox-sensitive molecule that serves an important role in mitochondrial functions. It participates in critical process such as electron shuttling through the electron transport chain, regulation of enzymatic activity, and synthesis of heme and iron-sulfur clusters[19,20]. Deregulation of iron metabolism and associated anemia has been associated with IBD[21]. The role that mitoNEET plays in the etiology of IBD remains to be determined.

CPEB4 gene encodes the cytoplasmic polyadenylation element-binding protein 4 (CEBP4), which belongs to a family of proteins that bind mRNAs and contain a cytoplasmic polyadenylation element (CPE) in their 3′-UTR. Binding results in 3′-

poly(A) tail extension and translational upregulation of target mRNAs. *Cpeb4* mRNA is rhythmically regulated in mouse liver, conferring temporal translational regulation. In the absence of CPEB4, a large number of mRNAs are transcribed, but remain untranslated until needed[22]. A recent study, using knockout mice models, showed that CPEB4 was required for translation of numerous proteins involved in ER homeostasis and CPEB4 loss resulted in mitochondrial dysfunction and defective lipid metabolism, two hallmarks of ER stress. *Cpeb4* KO livers were highly susceptible to ER stress-induced apoptosis and to development of NAFLD[23]. In CD, reduced CPEB4 may also lead to ER stress and mitochondrial dysfunction.

DOCK7 encodes dedicator of cytokinesis 7 protein (Dock7), a member of Dock proteins family and an activator of Rac GTPases. DOCK7 plays an important role in axon outgrowth, Schwann cell migration, and axon myelination[24]. Mutation in this gene in mice leads to hypopigmentation suggesting a non-redundant role in the distribution and function of dermal and follicular melanocytes. However, mutant mice show normal neuronal function despite the high expession of DOCK7 in the developping brain, suggesting redundancy with other Docks[25]. The role of DOCK7 in IBD and immune cells function is totally unknown.

ERAP2 gene encodes an endoplasmic reticulum aminopeptidase (ERAP2), an enzyme involved in trimming of peptides for MHC-I loading. Aberrant ERAP2 function could influence peptide-HLA-B27 stability, formation of MHC-I free heavy chains and ER stress[26,27,28]. SNPs in *ERAP2* gene have been associated with CD[29]. Although the underlying mechanisms are not known, it is possible that ERAP2 modification contributes to the reported reduction of MHCI on CD4 T cells from CD patients[30]. ERAP2 modification may also contribute to the epithelial ER stress associated with CD and UC.

GNA12 encodes Guanine nucleotide-binding protein subunit alpha-12 or $G\alpha_{12}$, which belongs to the heterotrimeric G proteins. $G\alpha_{12}$ is found in tight junctions (TJ) where it interacts with ZO-1[31] and plays important roles in para-cellular permeability[32,33]. $G\alpha_{12}$ is ubiquitously expressed and interacts, upon receptor-mediated activation, with certain Rho guanine nucleotide exchange factors (RhoGEFs) which in turn mediate activation of the small GTPase RhoA[34]. Intestinal

permeability and barrier dysfunction is a hallmark of CD and UC. Several studies reported changes in the expression of several TJ proteins in both diseases[35]. It is conceivable that modifications in the $G\alpha_{12}$ pool leads to alteration of intestinal permeability. Tissue-specific $G\alpha_{12}$-deficient mice revealed important functions of this protein in modulating T cell trafficking and proliferation, as well as in the response to foreign and self antigens[36], important processes that may affect susceptibility for T cell-mediated diseases.

GPX1 encodes the glutathione peroxidase 1 (GPX1), a highly abundant and ubiquitously expressed cytosolic enzyme. Like all glutathione peroxidases family members, GPX1 catalyzes the reduction of H2O2 by glutathione and consequently, protects cells from oxidative damage. In IBD, it is believed that intestinal and colonic injuries and dysfunction is at least partially due to elevation of reactive metabolites of oxygen and nitrogen[37]. Although the role of GPX1 is not known in IBD, deficiency of both GPX1 and GPX2 in mice lead to spontaneous ileo-colitis and intestinal cancer[38]. A protective role of GPX1 and GPX2 against oxidative stress has also been suggested by studies reporting elevated *Gpx1/2* gene expression in gastric mucosa after *H. pylori* infection[39]. Association of the elevated expression of *Gpx1/2* gene with tumorigenesis could be due to its anti-apoptotic activity[40].

GSDMB encodes Gasdermin-B protein (GSDMB) the function of which is largely unknown. The expression of *GSDMB* has been associated with differentiated epithelial cells and with regions containing proliferating cells or stem cells, respectively, of the esophagus and the gastric mucosa[41,42].

JAZF1, also known as *TIP27*, encodes a transcriptional repressor of *NR2C2*, also known as *TAK1* or *TR4*[76]. Mice deficient in *NR2C2* show low IGF1 serum concentrations and perinatal and early postnatal hypoglycemia, as well as growth retardation[77]. *JAZF1* also affects variation in human height[78]. SNPs in *JAZ1F* have been associated with type II diabetes[79], prostate[80] and endometrial cancer[81] and with systemic lupus erythematosus[82]. However, the role of *JAZF1* in immune response and autoimmunity remains to be elucidated.

LSP1 encodes a leukocyte-specific protein 1 (LSP1), a Ca^{2+}-activated, intracellular

filamentous actin-binding protein that interacts with the cytoskeleton and is expressed in hematopoietic lineage and in endothelial cells[70]. Evidence from mice model studies suggest that LSP1 plays a negative regulatory role on neutrophil and T cell migration[71,72]. A recent study identified a novel *LSP1* deletion variant for RA susceptibility through CNV GWAS[73]. The copy number of *LSP1* was found to be significantly lower in RA patients and was associated with increased T cell migration[73]. We found a positive correlation of LSP1 expression (in $CD14^+$ cells) with UC, but not with CD. UC, as well as CD, is characterized by an increased infiltration of immune cells in inflamed tissues. Our finding is therefore surprising if we consider the concept of an association between increased cell migration with *LSP1* CNVs and LSP1 insufficiency. It is possible that LSP1 plays an additional, yet unknown role in monocytes. On the other hand, if LSP1 participates actively in the cross-talk between leukocytes and endothelial cells during leukocyte transmigration, the physiological differences in microvasculature and the integrins involved may dictate organ-specific roles for LSP1 in leukocyte recruitment into the inflammatory sites.

NXPE1: Encodes Neuroexophilin and PC-esterase domain family member 1 (NXPE1). A human gastointestinal tract (GIT) specific transcriptome and proteome study validate the expression pattern of this gene and protein in the intestine [74]. NXPE1 was recently identified as a novel target gene for IBD-associated variants[75]. Its function remains largely unknown.

ORMDL3 encodes ORM1-like protein 3, a negative regulator of sphingolipid synthesis and a regulator of endoplasmic reticulum-mediated calcium signaling[45]. ORMDL3 is involved in the regulation of eosinophil and T cell functios[46,47]. It also facilitate B cells survival and regulates autophagy through the ATF6 signaling pathway[48]. Genetic variants regulating ORMDL3 expression have been associated with susceptibility to ashma[49], T1D[50], atherosclerosis[51], ankylosing spondylitis[52] and IBD[53]. ORMDL3 might be associated with IBDs and other autoimmune and inflammatory diseases by activating ERS, inducing autophagy and/or promoting immune cells activation.

REXO2 encodes an oligoribonuclease protein. Its depletion, using RNAi, causes a significant decrease of mtDNA and mtRNA and impaired *de novo* mitochondrial protein synthesis[83]. REXO2's function remains unknown but it may be involved in the well documented mitochondrial defects associated with IBD[84].

RNASET2 is the only RNase T2 family member in humans and is potentially involved in the inhibition of tumorigenesis, metastasis and angiogenesis[85,86]. Loss-of-function of RNASET2 protects fibroblasts from oxidative stress[89] while its overexpression in melanocytes and keratinocytes sensitizes these cells to oxidative-stress-induced apoptosis[90]. Interestingly, CD is characterized by an impaired immune cells apoptosis associated with elevated H_2O_2 in PBMC during the active phase of the disease[91]. Although speculative, it is possible that reduced *RNASET2* contributes to the altered oxidative stress in CD.

SKAP2 encodes the Src kinase-associated phosphoprotein 2 (Skap2), a cytosolic adaptor protein expressed in a variety of cell types including hematopoietic cells[54,55,56]. Skap2 has been implicated in cell adhesion through association to integrins and cytoplasmic actin[55], and is required for global actin reorganization. It interacts with different molecules implicated in integrin signaling events[54,56,57]. Loss of Skap2 in mice results in reduced inflammation in experimental autoimmune encephalomyelitis as well as defects in macrophage migration into tumor metastasis, suggesting a physiologically important role of Skap2 for leukocyte recruitment *in vivo*[55,58].

UBE2L3 gene encodes an atypical Ubiquitin E2 Conjugase (UBE2L3) the role of which has been recently uncovered. It is an indirect human and mouse Caspase-1 target and plays an important role in the maturation of IL-1β. UBE2L3 depletion in mice increases pro-IL-1β levels and mature-IL-1β secretion by inflammasomes[61]. Several GWAS identified polymorphisms in the genomic locus of *UBE2L3* that are associated with multiple autoimmune diseases[62] including CD[29]. Decreased secretion of the inflammasome cytokine IL-1β was noted in monocytes of Crohn's disease patients[63]. It is therefore tempting to speculate that *UBE2L3* contributes to disease at least partially by modulating IL-1β secretion.

ZMIZ1 encodes Zmiz1, a member of the protein inhibitor of activated STAT (PIAS)-like family of coregulators[64]. Zmiz1 is widely and variably expressed[65]. In GWAS, a SNP within ZMIZ1 gene was associated with early-onset Crohn's disease and IBD[66]. *ZMIZ1* is co-expressed with activated *NOTCH1* across a broad range of T-ALL oncogenomic subgroups. Its inhibition slows human T-ALL cell proliferation and/or sensitizes them to γ-Secretase inhibitors (GSI)[67]. Evidence from Zmiz1-deficient mice demonstrated that Zmiz1 is a direct Notch1 cofactor that heterogeneously regulates Notch1 target genes and plays an important role in T cells development[68]. Altered expression of *ZMIZ1* has been reported to affect Smad3-mediated transcription[69]. Interestingly, our analysis shows that increased UC disease risk was associated with decrease of both *SMAD3* and *ZMIZ1* expression while no association was observed with *NOTCH1*. This association was observed in different tissues/cell types suggesting a possible trans effect of *ZMIZ1* on *SMAD3* expression.

Supplementary Table 1

Cell type	Naive (r^2 based)			Frequentist (Nica et al., 2010)			Theta-based		
	Overlaps observed	Overlaps expected	P value	Overlaps observed	Overlaps expected	P value	Overlaps observed	Overlaps expected	P value
CD4	12	3.3	< 0.01	14	4.9	< 0.01	17	8.4	< 0.01
CD8	12	3.5	< 0.01	18	4.3	< 0.01	16	6.9	< 0.01
CD14	8	3.3	0.061	9	4.7	0.211	10	7.1	0.720
CD15	4	1.9	0.646	4	2	0.720	7	5.1	0.909
CD19	7	2	0.010	7	3.6	0.410	12	5.8	0.044
PLA	4	0.9	0.010	3	0.9	0.475	5	1.8	0.119
IL	4	1.6	0.432	7	2.1	0.027	8	4.1	0.281
TR	6	2.6	0.211	5	3.5	0.928	11	6	0.086
RE	5	1.5	0.103	6	2.4	0.204	9	5.5	0.509

Enrichment of DAP-EAP matching in 63 of 97 CD risk loci covered by the Immunochip. For each cell type, we provide the number of matches (or overlaps) observed with the top disease-associated SNPs (MAF > 0.05), as well as the number of matches expected with the same number of SNPs (MAF > 0.05) sampled at random in the same 63 risk loci. The analyses were conducted using three "colocalisation" methods (Naive, Frequentists and Theta-based). The p-values were determined by simulation (1,000 sets of 63 randomly sampled SNPs) and Bonferroni corrected for the analysis of 9 cell types. < 0.01 means that the number of matches observed with the real disease-associated SNPs was never observed with any set (out of 1,000) of randomly sampled SNPs.

214 **Supplementary Table 2**

215

Tissue	Nr of samples	Nr of probes	Nr of PCs
CD4	303	13,466	38
CD8	294	13,317	35
CD19	282	12,648	40
CD14	286	13,170	36
CD15	289	11,069	27
PLA	251	6,565	23
IL	200	15,401	59
TR	271	15,082	50
RE	267	14,844	53

216

217 Number of usable samples, probes and PC for each tissue type.

218

Supplementary Table 3

Tissue	Nr of probes	FDR≤0.25	FDR≤0.10	FDR≤0.05	FDR≤0.01
CD4	13,466	7,417	4,957	4,176	3,247
CD8	13,317	6,760	4,309	3,599	2,779
CD19	12,648	4,984	3,138	2,549	1,953
CD14	13,170	7,118	4,728	3,961	3,106
CD15	11,069	3,611	2,396	1,983	1,512
PLA	6,565	1,404	996	854	653
IL	15,401	2,769	1,728	1,426	1,031
TR	15,082	5,183	3,391	2,807	2,160
RE	14,844	4,180	2,726	2,295	1,731

Number of cis-eQTL found in the nine analyzed cell types for different FDR thresholds (see also Suppl. Figure 7).

Supplementary Figures

1. Supplementary Figure 1

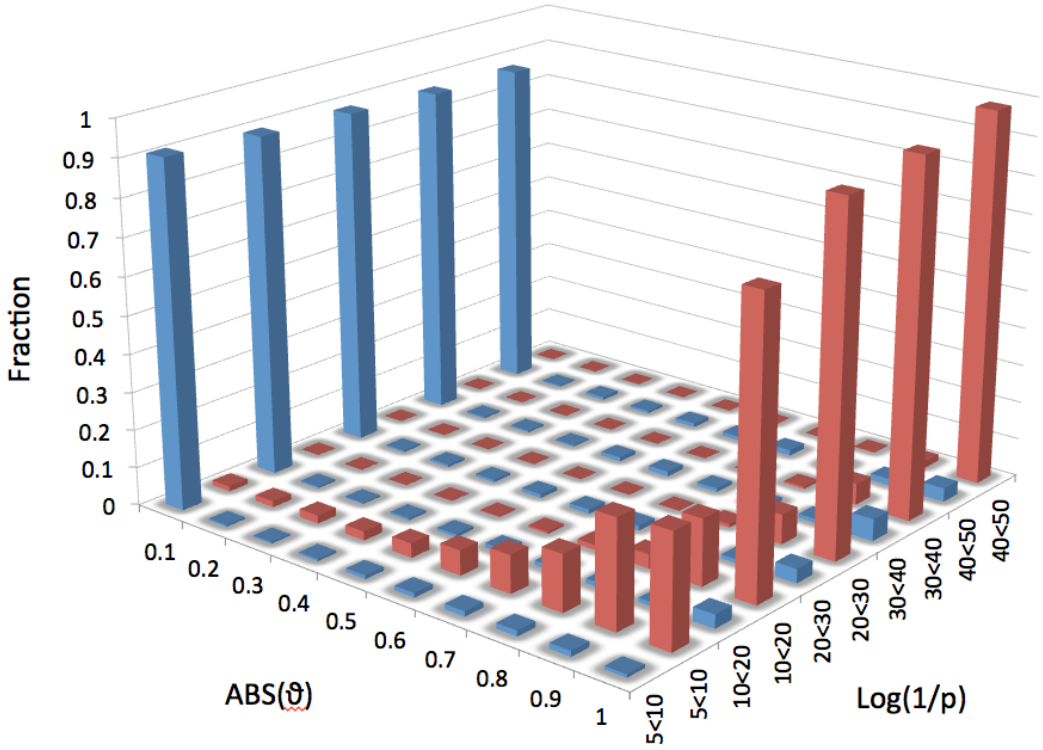

Absolute values of ϑ for pairs of eQTL driven by distinct regulatory variants (blue), and for pairs of eQTL driven by the same regulatory variants (red). The first (blue) were obtained by confronting real cis-eQTL with in silico simulated eQTL explaining the same variance as the real eQTL but driven by a randomly chosen SNPs in a 2Mb window centered around the probe. The second (red) were obtained by confronting eQTL obtained by reanalyzing two mutually exclusive halves of the CEDAR population separately in a region harboring a real cis-eQTL. It can be seen that ϑ very effectively discriminates between pairs of eQTL driven by distinct (blue) vs the same (red) regulatory variants. By choosing 0.6 as threshold value for ϑ, one captures most red pairs (~88%) with minimum contamination of blue pairs (~5%). Log(1/p): eQTL are sorted by the smallest log(1/p) value of the two eQTL being compared.

2. Supplementary Figure 2

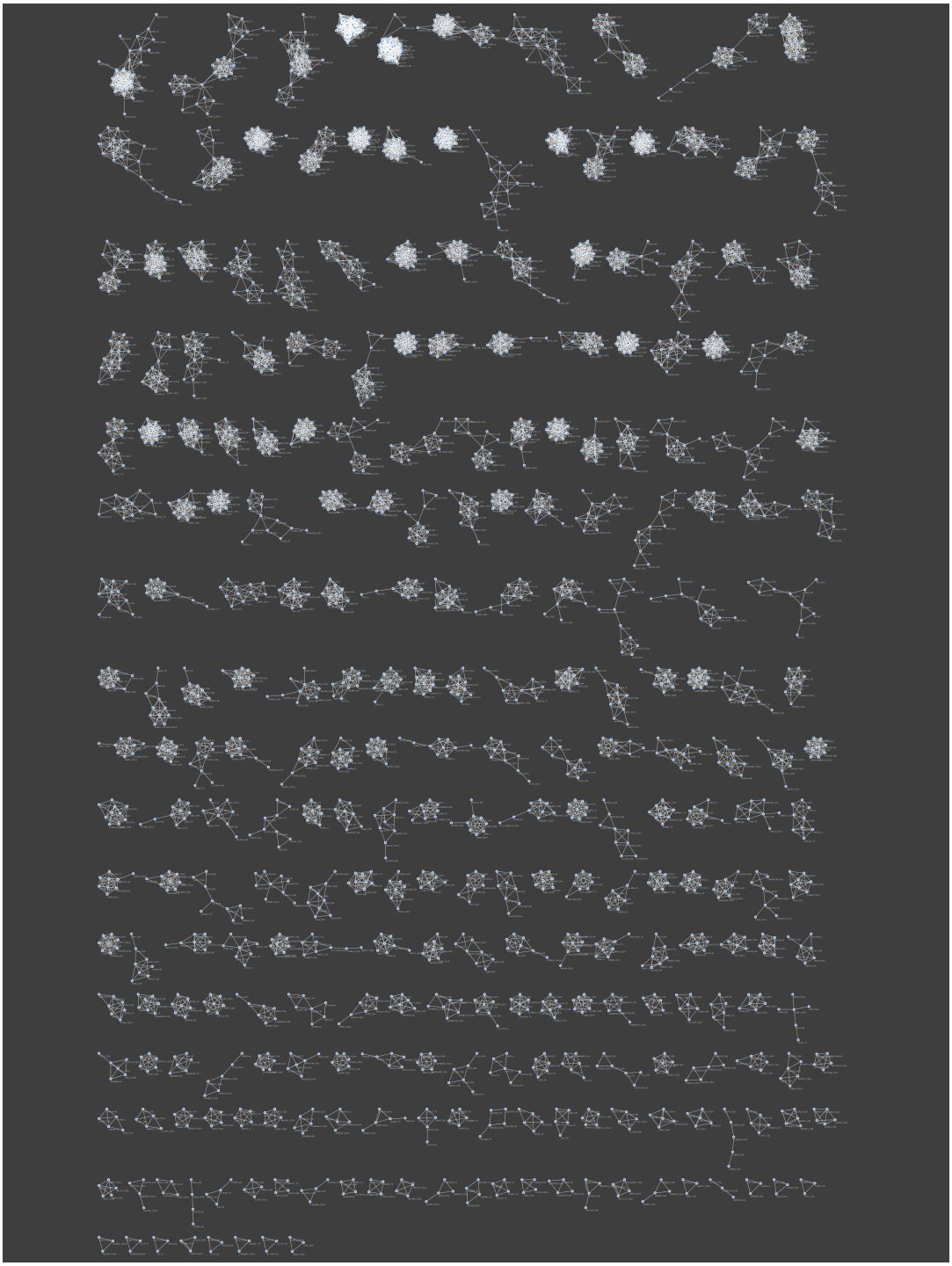

Graphical representation (using Cytoscape[1]) of 269 cis acting regulatory modules (cRM) including at least three genes (see Suppl. Table 2). Every node corresponds to a cis-eQTL involving a specific gene-tissue combination. Edges connect pairs of cis-eQTL for which $|\vartheta| \geq 0.6$.

1. Shannon, P. et al. Genome Res. 13, 2498-2504 (2003).

3. Supplementary Figure 3

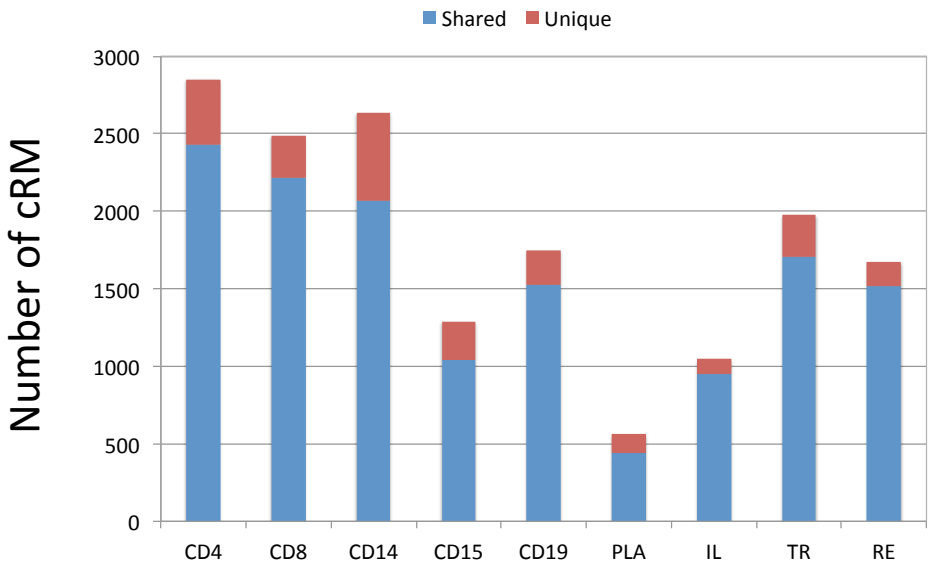

Number of cRM detected in each cell type. Blue: shared cRM (i.e. also detected in at least one other cell type). Red: Unique (i.e. detected only in that cell type).

4. Supplementary Figure 4

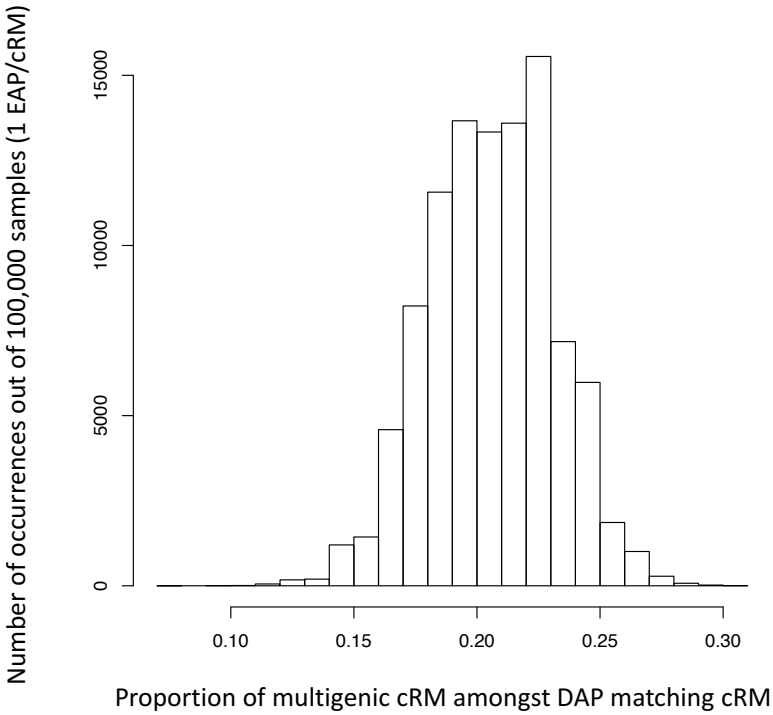

Across the entire genome, the proportion of multigenic cRM was shown to be 0.10 (see also main text, figure 1B). Amongst DAP matching cRM (mapping to 63 of 200 studied IBD risk loci; main text Table 1) this proportion was shown to be 0.33, hence a highly significant enrichment. To ensure that this enrichment was not only due to the fact that matching between DAP and EAP was de facto tested multiple times for multigenic cRM and only once for other cRM, we only tested one randomly sampled EAP per cRM (whether monogenic or multigenic). This was repeated 100,000 times and yielded the distribution of the proportion of multigenic cRM amongst DAP matching cRM shown above. The average was 0.22, and we never observed values ≤ 0.11, i.e. the genome-wide average.

5. Supplementary Figure 5

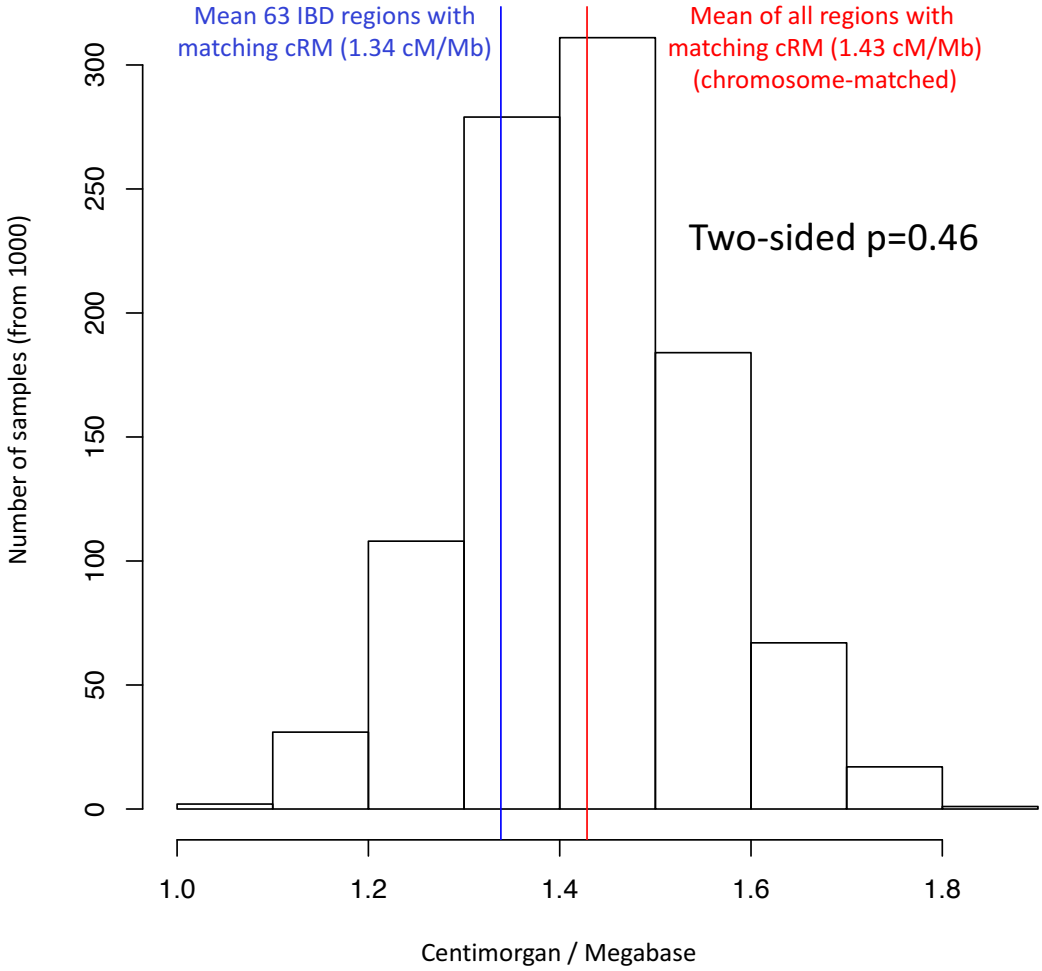

The 63 IBD risk loci with matching cRM are 2- to 3-fold enriched in multigenic cRM ($p \leq 10^{-5}$). This could be due to the fact that the LD is higher in IBD regions than in the rest of the genome. To test this, we downloaded LD-based recombination maps of the human genome from https://github.com/joepickrell/1000-genomes-genetic-maps. The average recombination rate across the human genome was 1.23 centimorgan per megabase (cM/Mb). The average recombination rate for the 63 IBD risk loci with matching cRM was 1.34 cM/Mb, i.e. less LD than in the rest of the genome. Regions encompassing eQTL (and hence cRM) may differ from the rest of the genome with regards to LD. Thus, we further sampled 1,000 sets of 63 loci centered on cRM (from our list of 9,720) that were matched for size and chromosomal location with the 63 cRM-matching IBD risk loci. The mean recombination rate for the cRM-centered genome was 1.43 cM/Mb. The figure shows the frequency distribution of the corresponding mean cRM/Mb per set (black), the mean of means of the 1,000 sets of 63 randomly drawn loci (red), and the mean of the 3 IBD risk loci (blue). The mean of the 63 IBD risk loci did not differ significantly from the rest of the cRM centered portion of the genome (two-tailed p-value: 0.46).

6. Supplemental Figure 6

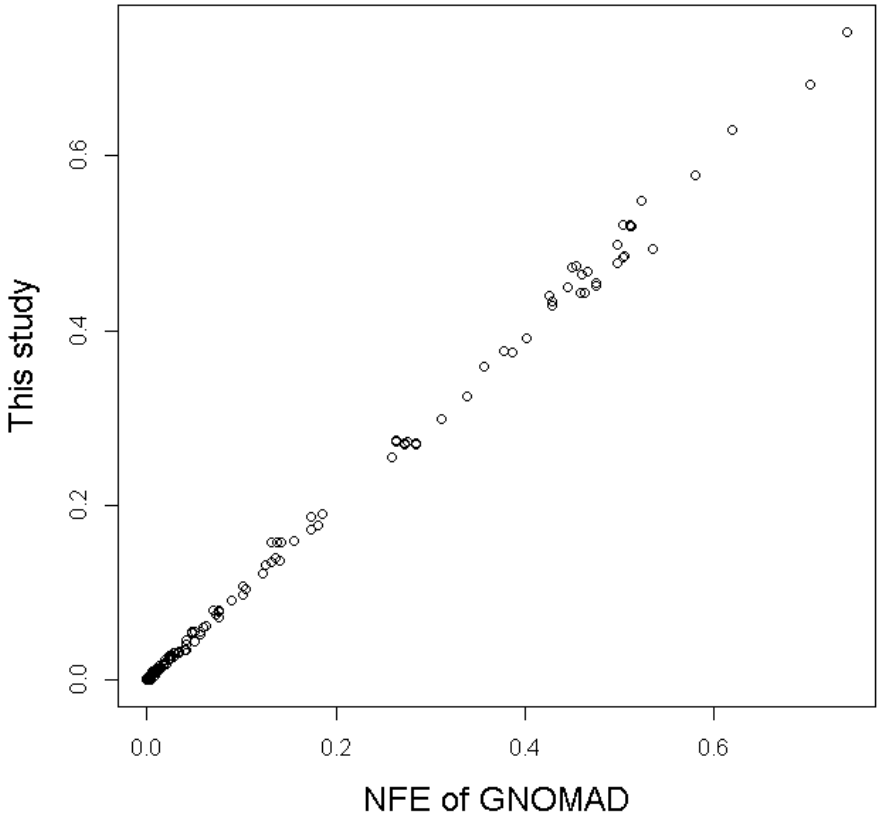

Comparison of the alternative allele frequency for 1,781 variants observed in this study and in 55,860 non-Finnish European samples from the GNMAD study.

7. Supplementary Figure 7

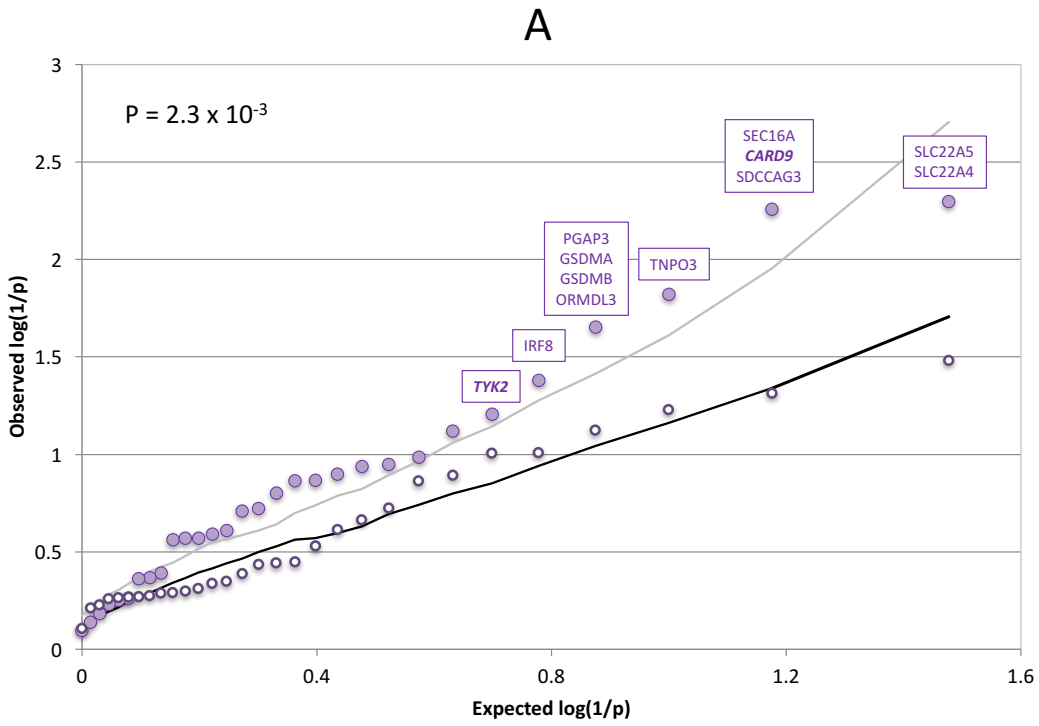

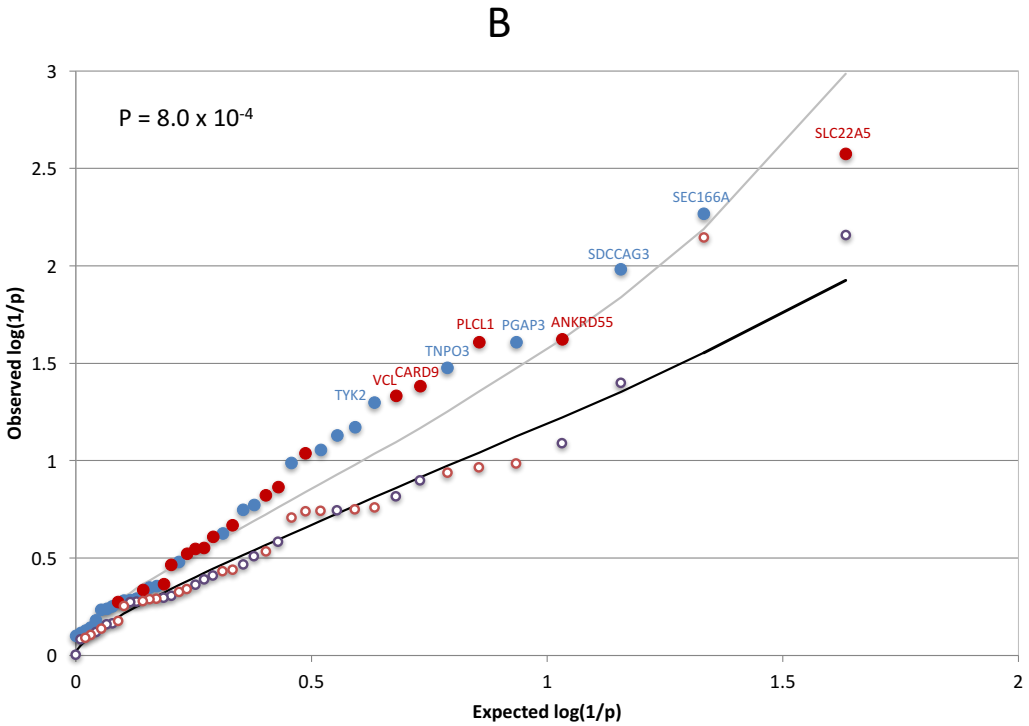

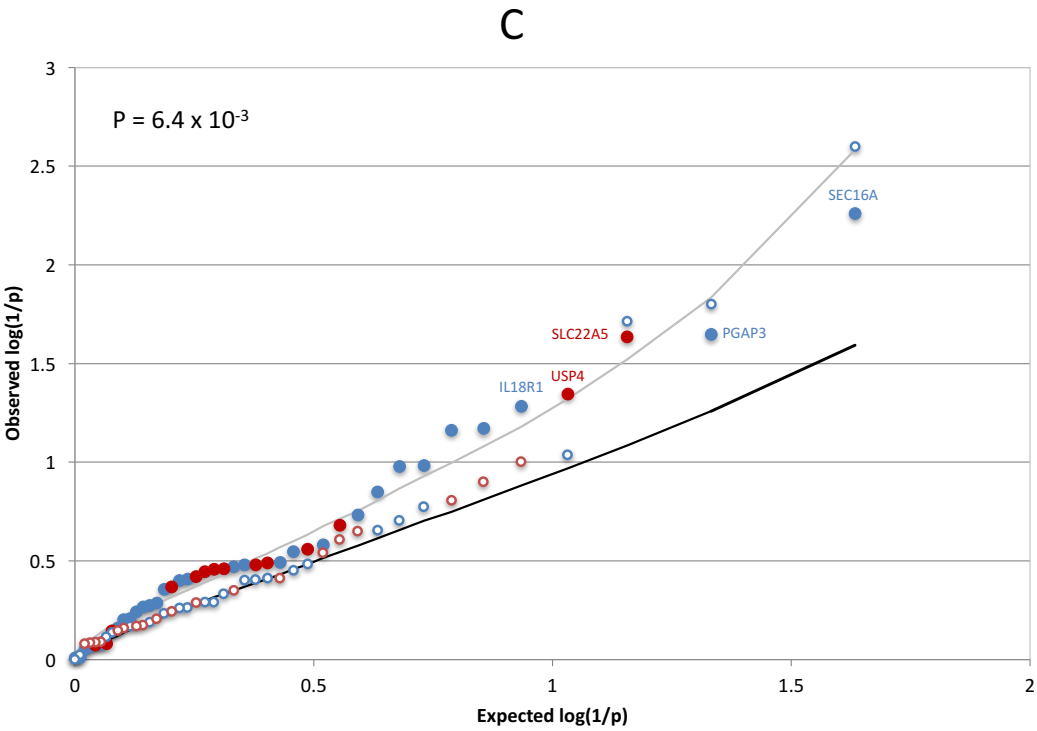

QQ-plot for the module-based burden test (**A**), disease plus age-of-onset-based burden test (**B**), and disease plus familiality-based burden test (**C**). Ranked log(1/p) values obtained when considering LoF and damaging variants (full circles), or synonymous variants (empty circles). The circles are labeled in blue when the best p-value for that gene is obtained with CAST, in red when the best p-value is obtained with SKAT, or in purple for the module-based test (as some genes in the module may have their best p-value with CAST and other with SKAT). The black line corresponds to the median log(1/p) value obtained (for the corresponding rank) using the same approach on permuted data (LoF and damaging variants). The grey line marks the upper limit of the 95% confidence band. The name of the genes/modules exceeding the nominal p-value of 0.05 are given. The inset p-values correspond to the significance of the upwards shift in log(1/p) values estimated by permutation.

8. Supplementary Figure 8

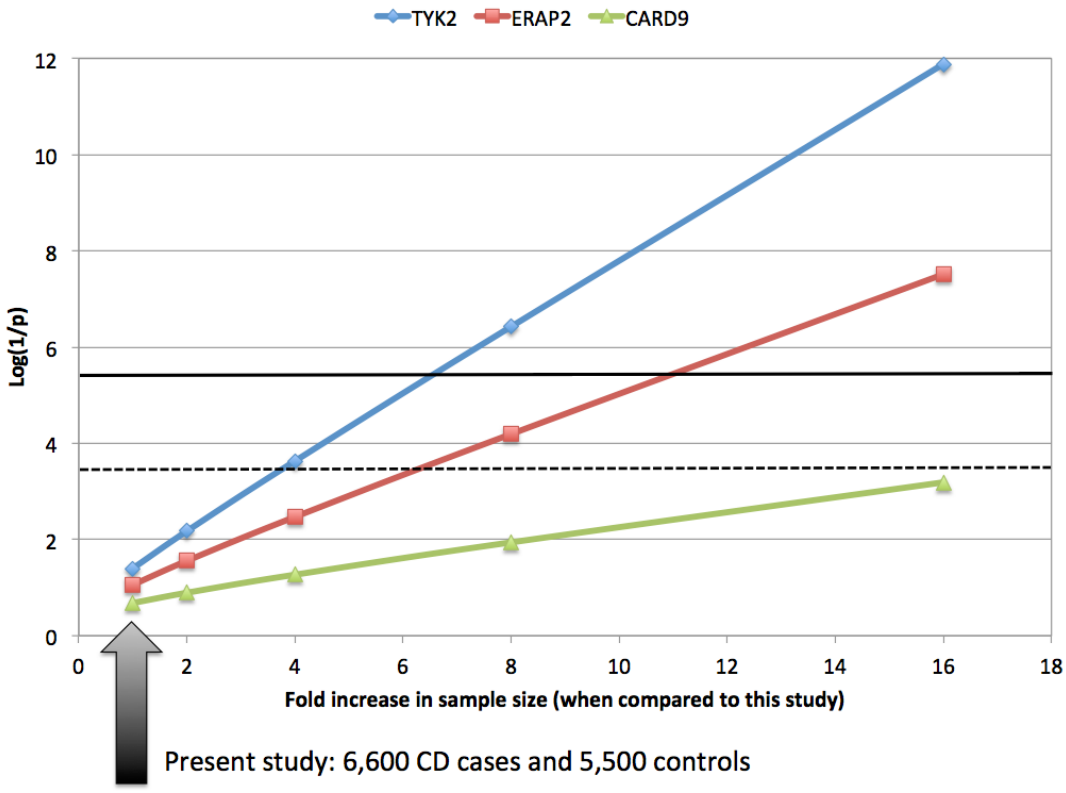

Effect of increasing sample size on the *log(1/p)* values of a one-sided burden test assuming that the effects observed for *TYK2* (blue), *ERAP2* (red) and *CARD9* (green) observed in this study are real unbiased. The dotted horizontal black line corresponds to an hypothetical experiment-wide significance threshold assuming the realization of 200 independent tests (targeting for instance 100-200 genes selected on the basis of coincident DAP-EAP patterns). The plain horizontal black line corresponds to an hypothetical genome-wide significance threshold assuming the realization of 20,000 independent tests (targeting all genes). It can be seen that an at least 4-fold increase in sample size is needed to achieve significance in the first scenario and at least 7-fold increase in the second scenario.

9. Supplementary Figure 9

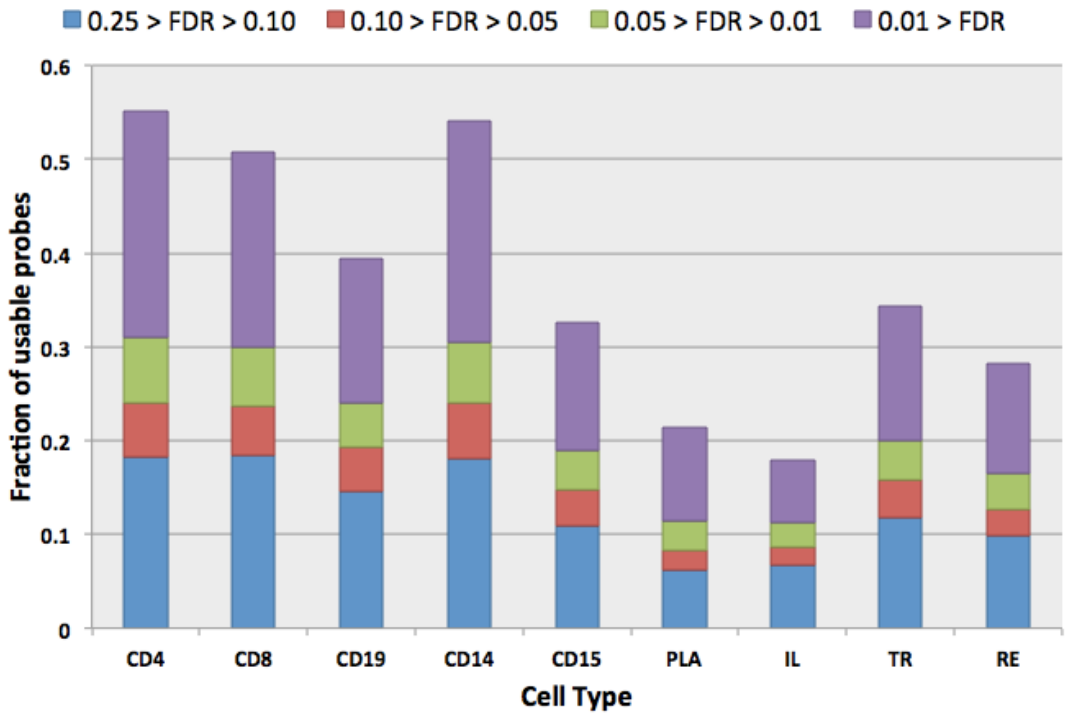

Proportion of usable probes with cis-eQTL at various levels of FDR in the nine analyzed cell types.

10. Supplementary Figure 10

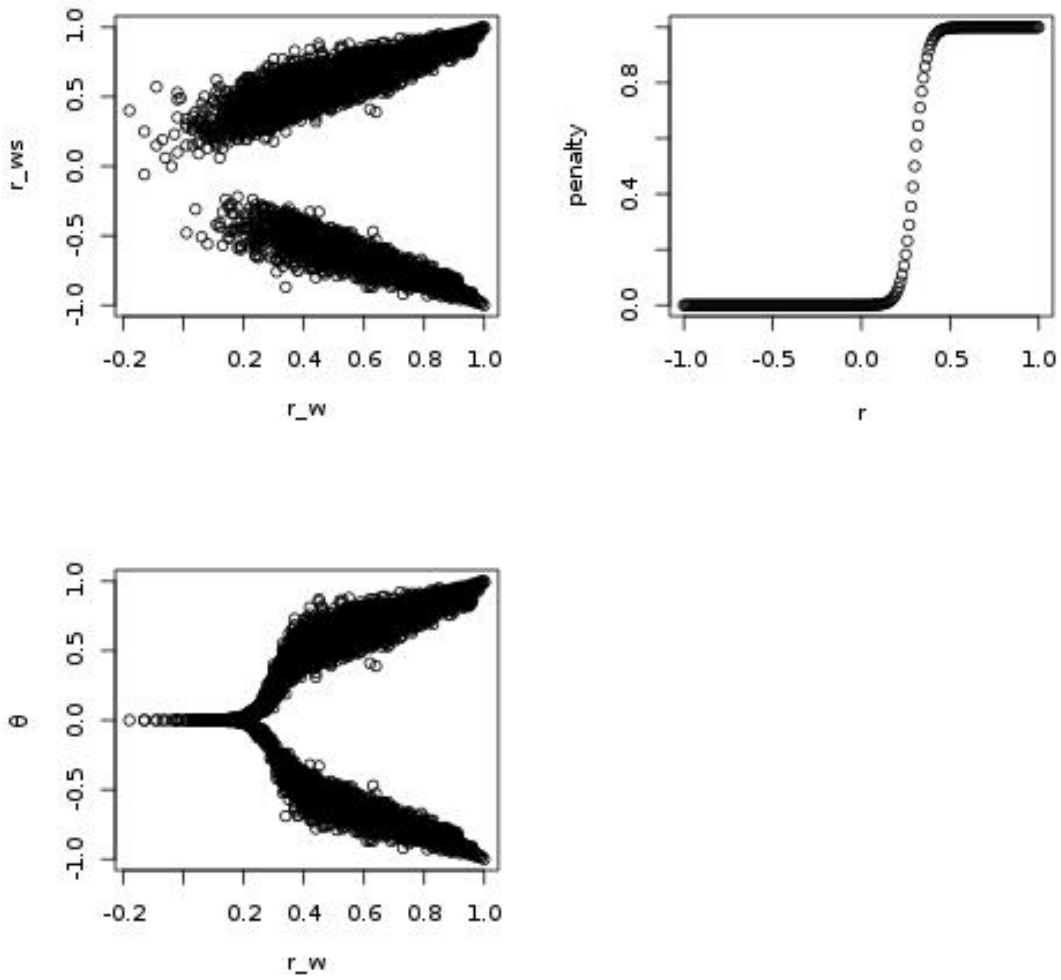

Graphical illustration of the relationship between r_w, r_{ws} and ϑ. The penalty function applied to r_{ws} to generate ϑ, corresponds to $\frac{1}{1+e^{-k(r_w-T)}}$.. The graph is shown for k = 30 and T=0.3, the values used in this study.

The point here is that if two association patterns are "similar" (driven by the same variants), the correlation (r_w in Suppl. Methods) between –log(1/p) values is expected to be positive. If two association patterns are different (driven by distinct variants) they may generate strong negative correlations (r_w). The first part of the method aims at weeding out such instances (negative r_w). One way to do this is to choose a simple threshold value for r_w. We herein propose an approach that offers more flexibility: it generates a penalty that increases when the correlation decreases with an adaptable rate. As shown in Suppl. Fig. 8, the values of k=30 and T=0.3 essentially correspond to a threshold value of 0.3. As can also be seen from Suppl. Fig. 8, there is (as expected) a strong linear relationship with slope 1 between r_w and $|r_{ws}|$ (and hence between r_w and $|\vartheta|$ for pairs with $r_w > 0.3$). Because we subsequently use a threshold value $|\vartheta| \geq 0.6$, the choice T has very little impact on the outcome unless one approaches 0.6.

11. Supplementary Figure 11

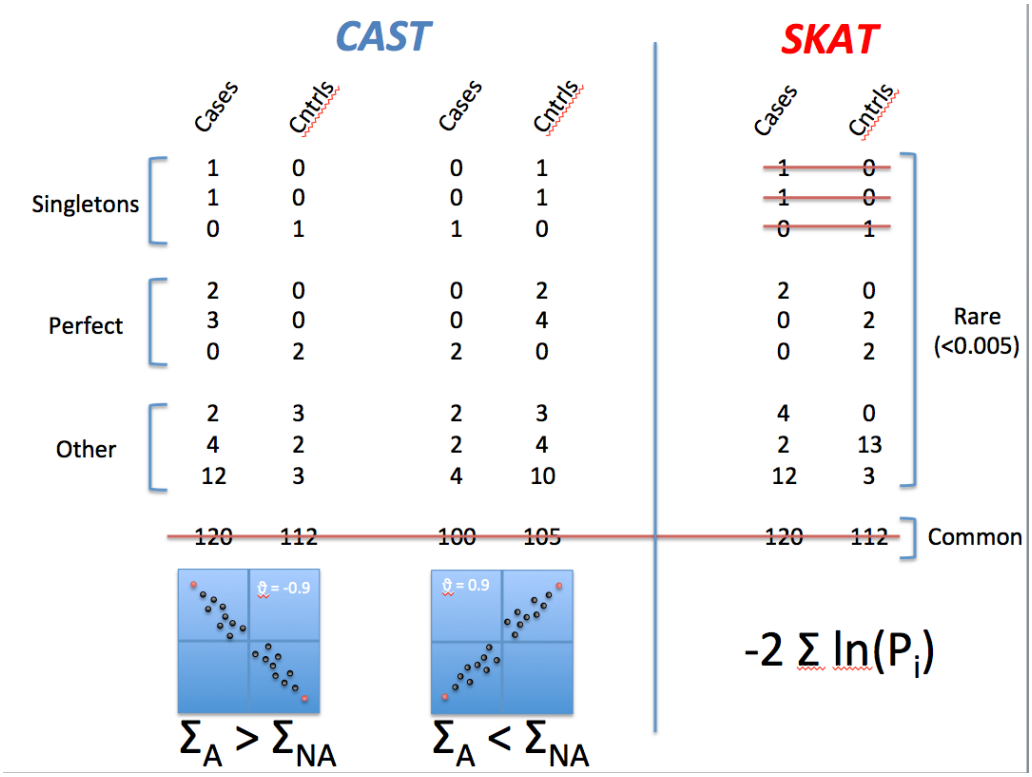

Schematic representation of the key features of the implemented "burden test".

The analysis is restricted to rare variants with MAF < 0.005 to ensure that the new signal is independent of the one that lead to the identification of the corresponding risk loci by GWAS (based on common and low frequency variants). Variants can be sorted in (i) singletons (i.e. observed only ones in the analyzed samples), (ii) perfect (i.e. observed more than ones in the sample but perfectly associated with disease status), and (iii) other (i.e. observed more than ones in the sample in both cases and controls).

We test two hypotheses. The first assumes that disruptive variants are either enriched in cases or in controls as a function of the sign of the correlation between DAP and EAP (if decreased expression is associated with increased risk, disruptive "risk" variants are expected to be enriched in cases; if increased expression is associated with increased risk, disruptive "protective" variants are expected to be enriched in controls). The test is implemented with CAST and in essence performs a one-sided test of independence (what is the probability to observe the excess of disruptive variants in cases (respectively controls) by chance alone?). The second hypothesis tests whether the distribution of the variants in cases and controls is characterized by too many variants that tend to be overrepresented either in cases or in controls. Thus, this hypothesis allows some disruptive variants to increase risk and others to be protective. This hypothesis does not use information from singletons. Testing this hypothesis is implemented with SKAT. It can be seen in simplified form as combining the p-values (from a test of independence) across variants (without considering the sign of the effect) using for instance Fisher's method.

12. Supplementary Figure 12

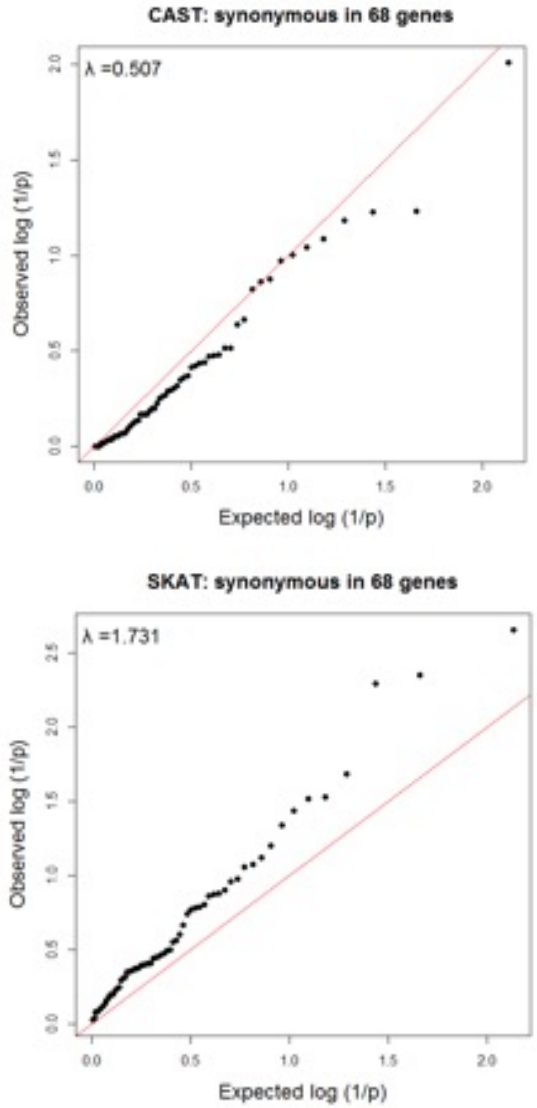

Distribution of permutation-based –log(p) values obtained for 68 analyzed genes with synonymous variants using CAST (A), and SKAT (B), indicating that CAST is conservative (, while SKAT is too permissive ($\lambda_{GC} = 1.73$). The 68 genes correspond to the 47 genes reported in this study, plus 21 genes sequenced in the same cohort as part of another study.

410

411 1. Dinarello, C. A., Novick, D., Kim, S. & Kaplanski, G. Interleukin-18 and IL-18
412 binding protein. *Frontiers in Immunology* **4,** (2013).

413 2. Elinav, E. *et al.* NLRP6 inflammasome regulates colonic microbial ecology and
414 risk for colitis. *Cell* **145,** 745–757 (2011).

415 3. Salcedo, R. *et al.* MyD88-mediated signaling prevents development of
416 adenocarcinomas of the colon: role of interleukin 18. *J. Exp. Med.* **207,** 1625–36
417 (2010).

418 4. Nowarski, R. *et al.* Epithelial IL-18 Equilibrium Controls Barrier Function in
419 Colitis. *Cell* **163,** 1444–1456 (2015).

420 5. Dinarello, C. A. Interleukin-18 and the Pathogenesis of Inflammatory Diseases.
421 *Semin. Nephrol.* **27,** 98–114 (2007).

422 6. Heinrich, P. C. *et al.* Principles of interleukin (IL)-6-type cytokine signalling and
423 its regulation. *Biochem. J.* **374,** 1–20 (2003).

424 7. Mitsuyama, K. *et al.* Therapeutic strategies for targeting the IL-6/STAT3
425 cytokine signaling pathway in inflammatory bowel disease. *Anticancer Res.* **27,**
426 3749–56

427 8. Atreya, R. *et al.* Blockade of interleukin 6 trans signaling suppresses T-cell
428 resistance against apoptosis in chronic intestinal inflammation: evidence in
429 Crohn disease and experimental colitis in vivo. *Nat. Med.* **6,** 583–588 (2000).

430 9. Ito, H. *et al.* A Pilot Randomized Trial of a Human Anti-Interleukin-6 Receptor
431 Monoclonal Antibody in Active Crohn's Disease. *Gastroenterology* **126,** 989–
432 996 (2004).

433 10. Jones, S. A., Scheller, J. & Rose-John, S. Therapeutic strategies for the clinical
434 blockade of IL-6/gp130 signaling. *J. Clin. Invest.* **121,** 3375–3383 (2011).

435 11. Lesourne, R. *et al.* Themis, a T cell-specific protein important for late thymocyte
436 development. *Nat. Immunol.* **10,** 840–7 (2009).

437 12. Fu, G. *et al.* Themis controls thymocyte selection through regulation of T cell
438 antigen receptor-mediated signaling. *Nat. Immunol.* **10,** 848–56 (2009).

439 13. Neurath, M. F. Cytokines in inflammatory bowel disease. *Nat. Rev. Immunol.* **14,**

329–342 (2014).

14. Palumbo, R. *et al.* APEH Inhibition Affects Osteosarcoma Cell Viability via Downregulation of the Proteasome. *Int. J. Mol. Sci.* **17,** 1614 (2016).

15. Cleynen, I. *et al.* Genetic and microbial factors modulating the ubiquitin proteasome system in inflammatory bowel disease. *Gut* **63,** 1265–74 (2014).

16. Li, J., Mahajan, A. & Tsai, M.-D. Ankyrin Repeat: A Unique Motif Mediating Protein−Protein Interactions †. *Biochemistry* **45,** 15168–15178 (2006).

17. International Multiple Sclerosis Genetics Consortium (IMSGC) *et al.* Analysis of immune-related loci identifies 48 new susceptibility variants for multiple sclerosis. *Nat. Genet.* **45,** 1353–60 (2013).

18. Viatte, S. *et al.* Genetic markers of rheumatoid arthritis susceptibility in anti-citrullinated peptide antibody negative patients. *Ann. Rheum. Dis.* **71,** 1984–90 (2012).

19. Wiley, S. E., Murphy, A. N., Ross, S. A., van der Geer, P. & Dixon, J. E. MitoNEET is an iron-containing outer mitochondrial membrane protein that regulates oxidative capacity. *Proc. Natl. Acad. Sci. U. S. A.* **104,** 5318–5323 (2007).

20. Geldenhuys, W. J., Leeper, T. C. & Carroll, R. T. mitoNEET as a novel drug target for mitochondrial dysfunction. *Drug Discovery Today* **19,** 1601–1606 (2014).

21. Goldberg, N. D. Iron deficiency anemia in patients with inflammatory bowel disease. *Clinical and Experimental Gastroenterology* **6,** 61–70 (2013).

22. Kojima, S., Sher-Chen, E. L. & Green, C. B. Circadian control of mRNA polyadenylation dynamics regulates rhythmic protein expression. *Genes Dev.* **26,** 2724–2736 (2012).

23. Maillo, C. *et al.* Circadian- and UPR-dependent control of CPEB4 mediates a translational response to counteract hepatic steatosis under ER stress. *Nat. Cell Biol.* **19,** 94–105 (2017).

24. Watabe-Uchida, M., John, K. A., Janas, J. A., Newey, S. E. & Van Aelst, L. The Rac Activator DOCK7 Regulates Neuronal Polarity through Local Phosphorylation of Stathmin/Op18. *Neuron* **51,** 727–739 (2006).

471 25. Blasius, A. L. *et al.* Mice with mutations of Dock7 have generalized
472 hypopigmentation and white-spotting but show normal neurological function.
473 *Proc. Natl. Acad. Sci.* **106,** 2706–2711 (2009).

474 26. Zhang, Z. *et al.* Functional interaction of ERAP2 and HLA-B27 activates the
475 unfolded protein response. *Arthritis Rheumatol.* (2016). doi:10.1002/art.40033

476 27. Andrés, A. M. *et al.* Balancing selection maintains a form of ERAP2 that
477 undergoes nonsense-mediated decay and affects antigen presentation. *PLoS*
478 *Genet.* **6,** 1–13 (2010).

479 28. Saveanu, L. *et al.* Concerted peptide trimming by human ERAP1 and ERAP2
480 aminopeptidase complexes in the endoplasmic reticulum. *Nat. Immunol.* **6,** 689–
481 97 (2005).

482 29. Franke, A. *et al.* Genome-wide meta-analysis increases to 71 the number of
483 confirmed Crohn's disease susceptibility loci. *Nat. Genet.* **42,** 1118–25 (2010).

484 30. Damjanovich, L., Volkó, J., Forgács, A., Hohenberger, W. & Bene, L. Crohn's
485 disease alters MHC-rafts in CD4 + T-cells. *Cytom. Part A* **81 A,** 149–164 (2012).

486 31. Dodane, V. & Kachar, B. Identification of isoforms of G proteins and PKC that
487 colocalize with tight junctions. *J. Membr. Biol.* **149,** 199–209 (1996).

488 32. Meyer, T. N., Schwesinger, C. & Denker, B. M. Zonula occludens-1 is a
489 scaffolding protein for signaling molecules: G??12 directly binds to the Src
490 homology 3 domain and regulates paracellular permeability in epithelial cells. *J.*
491 *Biol. Chem.* **277,** 24855–24858 (2002).

492 33. Sabath, E. *et al.* Gα12 regulates protein interactions within the MDCK cell tight
493 junction and inhibits tight-junction assembly. *J. Cell Sci.* **121,** 814–824 (2008).

494 34. Fukuhara, S., Chikumi, H. & Gutkind, J. S. RGS-containing RhoGEFs: the
495 missing link between transforming G proteins and Rho? *Oncogene* **20,** 1661–
496 1668 (2001).

497 35. Landy, J. *et al.* Tight junctions in inflammatory bowel diseases and inflammatory
498 bowel disease associated colorectal cancer. *World Journal of Gastroenterology*
499 **22,** 3117–3126 (2016).

500 36. Herroeder, S. *et al.* Guanine Nucleotide-Binding Proteins of the G12 Family
501 Shape Immune Functions by Controlling CD4+ T Cell Adhesiveness and

Motility. *Immunity* **30,** 708–720 (2009).

37. Pavlick, K. P. *et al.* Role of reactive metabolites of oxygen and nitrogen in inflammatory bowel disease 1,2 1This article is part of a series of reviews on 'Reactive Oxygen and Nitrogen in Inflammation.' The full list of papers may be found on the homepage of the journal. 2Gue. *Free Radic. Biol. Med.* **33,** 311–322 (2002).

38. Chu, F. F. *et al.* Bacteria-Induced Intestinal Cancer in Mice with Disrupted Gpx1 and Gpx2 Genes. *Cancer Res.* **64,** 962–968 (2004).

39. Maeda, S. *et al.* cDNA microarray analysis of Helicobacter pylori-mediated alteration of gene expression in gastric cancer cells. *Biochem. Biophys. Res. Commun.* **284,** 443–9 (2001).

40. Hockenbery, D. M., Oltvai, Z. N., Yin, X. M., Milliman, C. L. & Korsmeyer, S. J. Bcl-2 functions in an antioxidant pathway to prevent apoptosis. *Cell* **75,** 241–51 (1993).

41. Saeki, N. *et al.* GASDERMIN, suppressed frequently in gastric cancer, is a target of LMO1 in TGF-beta-dependent apoptotic signalling. *Oncogene* **26,** 6488–98 (2007).

42. Saeki, N. *et al.* Distinctive expression and function of four GSDM family genes (GSDMA-D) in normal and malignant upper gastrointestinal epithelium. *Genes, Chromosom. Cancer* **48,** 261–271 (2009).

43. Pal, L. R. & Moult, J. Genetic basis of common human disease: Insight into the role of missense SNPs from genome-wide association studies. *J. Mol. Biol.* **427,** 2271–2289 (2015).

44. Jostins, L. *et al.* Host-microbe interactions have shaped the genetic architecture of inflammatory bowel disease. *Nature* **491,** 119–24 (2012).

45. Breslow, D. K. *et al.* Orm family proteins mediate sphingolipid homeostasis. *Nature* **463,** 1048–1053 (2010).

46. Ha, S. G. *et al.* ORMDL3 promotes eosinophil trafficking and activation via regulation of integrins and CD48. *Nat. Commun.* **4,** 2479 (2013).

47. Schmiedel, B. J. *et al.* 17q21 asthma-risk variants switch CTCF binding and regulate IL-2 production by T cells. *Nat. Commun.* **7,** 13426 (2016).

533 48. Dang, J. *et al.* ORMDL3 Facilitates the Survival of Splenic B Cells via an
534 ATF6α-Endoplasmic Reticulum Stress-Beclin1 Autophagy Regulatory Pathway.
535 *J. Immunol.* (2017). doi:10.4049/jimmunol.1602124

536 49. Zhai, W. H., Song, C. Y., Huang, Z. G. & Sha, H. Correlation between the
537 genetic polymorphism of ORMDL3 gene and asthma risk: a meta-analysis.
538 *Genet. Mol. Res.* **14,** 7101–12 (2015).

539 50. Saleh, N. M. *et al.* Genetic association analyses of atopic illness and
540 proinflammatory cytokine genes with type 1 diabetes. *Diabetes. Metab. Res. Rev.*
541 **27,** 838–43 (2011).

542 51. Ma, X. *et al.* ORMDL3 contributes to the risk of atherosclerosis in Chinese Han
543 population and mediates oxidized low-density lipoprotein-induced autophagy in
544 endothelial cells. *Sci. Rep.* **5,** 17194 (2015).

545 52. Laukens, D. *et al.* Evidence for significant overlap between common risk
546 variants for Crohn's disease and ankylosing spondylitis. *PLoS One* **5,** e13795
547 (2010).

548 53. McGovern, D. P. B. *et al.* Genome-wide association identifies multiple
549 ulcerative colitis susceptibility loci. *Nat. Genet.* **42,** 332–7 (2010).

550 54. Asazuma, N. *et al.* Interaction of linker for activation of T cells with multiple
551 adapter protiens in platelets activated by the glycoprotein VI-selective ligand,
552 convulxin. *J. Biol. Chem.* **275,** 33427–33434 (2000).

553 55. Togni, M. *et al.* Regulation of In Vitro and In Vivo Immune Functions by the
554 Cytosolic Adaptor Protein SKAP-HOM. *Mol. Cell. Biol.* **25,** 8052–8063 (2005).

555 56. Alenghat, F. J. *et al.* Macrophages require Skap2 and Sirpα for integrin-
556 stimulated cytoskeletal rearrangement. *J. Cell Sci.* **125,** 5535–5545 (2012).

557 57. Königsberger, S. *et al.* HPK1 associates with SKAP-HOM to negatively regulate
558 Rap1-mediated B-lymphocyte adhesion. *PLoS One* **5,** 1–9 (2010).

559 58. Tanaka, M. *et al.* SKAP2 Promotes Podosome Formation to Facilitate Tumor-
560 Associated Macrophage Infiltration and Metastatic Progression. *Cancer Res.* **76,**
561 358–369 (2016).

562 59. Sartor, R. B. Mechanisms of disease: pathogenesis of Crohn's disease and
563 ulcerative colitis. *Nat. Clin. Pract. Gastroenterol. Hepatol.* **3,** 390–407 (2006).

564 60. Ghosh, S. *et al.* Natalizumab for active Crohn's disease. *N Engl J Med* **348,** 24–
565 32. (2003).

566 61. Eldridge MJ, Sanchez-Garrido J, Hoben GF, Goddard PJ, S. A. The Atypical
567 Ubiquitin E2 Conjugase UBE2L3 Is an Indirect Caspase-1 Target and Controls
568 IL-1β Secretion by Inflammasomes. *Cell Rep.* **18,** 1285–1297 (2017).

569 62. Alpi, A. F., Chaugule, V. & Walden, H. Mechanism and disease association of
570 E2-conjugating enzymes: lessons from UBE2T and UBE2L3. *Biochem. J.* **473,**
571 3401–3419 (2016).

572 63. Lamkanfi, M., Walle, L. Vande & Kanneganti, T. D. Deregulated inflammasome
573 signaling in disease. *Immunological Reviews* **243,** 163–173 (2011).

574 64. Shuai, K. & Liu, B. Regulation of gene-activation pathways by PIAS proteins in
575 the immune system. *Nat. Rev. Immunol.* **5,** 593–605 (2005).

576 65. Sharma, M. *et al.* hZimp10 is an androgen receptor co-activator and forms a
577 complex with SUMO-1 at replication foci. *EMBO J.* **22,** 6101–6114 (2003).

578 66. Imielinski, M. *et al.* Common variants at five new loci associated with early-
579 onset inflammatory bowel disease. *Nat. Genet.* **41,** 1335–40 (2009).

580 67. Rakowski, L. A. *et al.* Convergence of the ZMIZ1 and NOTCH1 Pathways at C-
581 MYC in Acute T Lymphoblastic Leukemias. *Cancer Res.* **73,** 930–941 (2013).

582 68. Pinnell, N. *et al.* The PIAS-like Coactivator Zmiz1 Is a Direct and Selective
583 Cofactor of Notch1 in T Cell Development and Leukemia. *Immunity* **43,** 870–
584 883 (2015).

585 69. Li, X., Thyssen, G., Beliakoff, J. & Sun, Z. The Novel PIAS-like Protein
586 hZimp10 Enhances Smad Transcriptional Activity. *J. Biol. Chem.* **281,** 23748–
587 23756 (2006).

588 70. Jongstra-Bilen, J. & Jongstra, J. Leukocyte-specific protein 1 (LSP1): a regulator
589 of leukocyte emigration in inflammation. *Immunol. Res.* **35,** 65–74 (2006).

590 71. Wang, C. *et al.* Modulation of Mac-1 (CD11b/CD18)-Mediated Adhesion by the
591 Leukocyte-Specific Protein 1 Is Key to Its Role in Neutrophil Polarization and
592 Chemotaxis. *J. Immunol.* **169,** 415–423 (2002).

593 72. Wang, J. *et al.* Accelerated wound healing in leukocyte-specific, protein 1-
594 deficient mouse is associated with increased infiltration of leukocytes and

595 fibrocytes. *J. Leukoc. Biol.* **82,** 1554–63 (2007).

596 73. Hwang, S.-H. *et al.* Leukocyte-specific protein 1 regulates T-cell migration in
597 rheumatoid arthritis. *Proc. Natl. Acad. Sci.* **112,** E6535–E6543 (2015).

598 74. Gremel, G. *et al.* The human gastrointestinal tract-specific transcriptome and
599 proteome as defined by RNA sequencing and antibody-based profiling. *J.*
600 *Gastroenterol.* **50,** 46–57 (2015).

601 75. Hulur, I. *et al.* Enrichment of inflammatory bowel disease and colorectal cancer
602 risk variants in colon expression quantitative trait loci. *BMC Genomics* **16,** 138
603 (2015).

604 76. Nakajima, T. TIP27: a novel repressor of the nuclear orphan receptor TAK1/TR4.
605 *Nucleic Acids Res.* **32,** 4194–4204 (2004).

606 77. Collins, L. L. *et al.* Growth retardation and abnormal maternal behavior in mice
607 lacking testicular orphan nuclear receptor 4. *Proc. Natl. Acad. Sci. U. S. A.* **101,**
608 15058–63 (2004).

609 78. Johansson, ??sa *et al.* Common variants in the JAZF1 gene associated with
610 height identified by linkage and genome-wide association analysis. *Hum. Mol.*
611 *Genet.* **18,** 373–380 (2009).

612 79. Cooper, J. D. *et al.* Meta-analysis of genome-wide association study data
613 identifies additional type 1 diabetes risk loci. *Nat. Genet.* **40,** 1399–401 (2008).

614 80. Thomas, G. *et al.* Multiple loci identified in a genome-wide association study of
615 prostate cancer. *Nat. Genet.* **40,** 310–5 (2008).

616 81. Koontz, J. I. *et al.* Frequent fusion of the JAZF1 and JJAZ1 genes in endometrial
617 stromal tumors. *Proc. Natl. Acad. Sci.* **98,** 6348–6353 (2001).

618 82. Martin, J. E. *et al.* A systemic sclerosis and systemic lupus erythematosus pan-
619 meta-GWAS reveals new shared susceptibility loci. *Hum. Mol. Genet.* **22,** 4021–
620 4029 (2013).

621 83. Bruni, F., Gramegna, P., Oliveira, J. M. A., Lightowlers, R. N. & Chrzanowska-
622 Lightowlers, Z. M. A. REXO2 is an oligoribonuclease active in human
623 mitochondria. *PLoS One* **8,** e64670 (2013).

624 84. Matondo, A. & Kim, S. S. Targeted-mitochondria antioxidants therapeutic
625 implications in inflammatory bowel disease. *J. Drug Target.* 1–8 (2017).

626 doi:10.1080/1061186X.2017.1339196

627 85. Acquati, F. *et al.* Microenvironmental control of malignancy exerted by
628 RNASET2, a widely conserved extracellular RNase. *Proc. Natl. Acad. Sci. U. S.*
629 *A.* **108,** 1104–9 (2011).

630 86. Acquati, F. *et al.* Loss of function of Ribonuclease T2, an ancient and
631 phylogenetically conserved RNase, plays a crucial role in ovarian tumorigenesis.
632 *Proc. Natl. Acad. Sci.* 1222079110- (2013). doi:10.1073/pnas.1222079110

633 87. Gabrielsen, I. S. M. *et al.* Genetic risk variants for autoimmune diseases that
634 influence gene expression in thymus. *Hum. Mol. Genet.* ddw152 (2016).
635 doi:10.1093/hmg/ddw152

636 88. Chu, X. *et al.* A genome-wide association study identifies two new risk loci for
637 Graves' disease. *Nat. Genet.* **43,** 897–901 (2011).

638 89. Caputa, G. *et al.* RNASET2 is required for ROS propagation during oxidative
639 stress-mediated cell death. *Cell Death Differ.* **23,** 347–57 (2016).

640 90. Wang, Q. *et al.* Stress-induced RNASET2 overexpression mediates melanocyte
641 apoptosis via the TRAF2 pathway in vitro. *Cell Death Dis.* **5,** e1022 (2014).

642 91. Moret-Tatay, I. *et al.* Possible Biomarkers in Blood for Crohn's Disease:
643 Oxidative Stress and MicroRNAs—Current Evidences and Further Aspects to
644 Unravel. *Oxid. Med. Cell. Longev.* **2016,** 1–9 (2016).

645